White, C. D., B. J. Willis, S. P. Dutton, J. P. Bhattacharya, and K. Narayanan, 2004, Sedimentology, statistics, and flow behavior for a tide-influenced deltaic sandstone, Frontier Formation, Wyoming, United States, *in* Integration of outcrop and modern analogs in reservoir modeling: AAPG Memoir 80, p. 129–152.

Sedimentology, Statistics, and Flow Behavior for a Tide-influenced Deltaic Sandstone, Frontier Formation, Wyoming, United States

Christopher D. White

The Craft and Hawkins Department of Petroleum Engineering, Louisiana State University, Baton Rouge, Louisiana, U.S.A.

Brian J. Willis

Department of Geology and Geophysics, Texas A&M University, College Station, Texas, U.S.A.

Shirley P. Dutton

Bureau of Economic Geology, John A. and Katherine G. Jackson School of Geosciences, University of Texas at Austin, Austin, Texas, U.S.A.

Janok P. Bhattacharya

Department of Geosciences, University of Texas at Dallas, Richardson, Texas, U.S.A.

Keshav Narayanan

Landmark Graphics Corp., Austin, Texas, U.S.A.

ABSTRACT

A study of a tide-influenced deltaic sandstone investigated geologic variations that affect hydrocarbon production in analogous reservoirs. The Cretaceous-aged Frewens Allomember was deposited by a delta prograding into a narrow shoreline embayment between an older, wave-dominated delta lobe to the south and a basin-floor ridge created by subtle structural uplift to the north. The Frewens Allomember is exposed in outcrops of the Frontier Formation in central Wyoming (United States). It comprises two 5-km-wide by 20-km-long upward-coarsening sandstone bodies. Each body contains basinward-dipping internal beds. Heterolithic beds capped by extensive shale drapes record episodic tidal deposition in the lower portions of the sandstone bodies, whereas sandier cross-stratified beds in the upper parts of bodies record stronger and more uniformly ebb-directed currents. During diagenesis, calcite concretions formed preferentially at the top of the upper sandstone body as water circulated down from overlying shales.

Diagrams of bedding, facies, calcite concretions, and bed-draping shales were compiled from high-resolution photomosaics and field observations. Sedimentologic logs, field permeameter measurements, and thin-section observations describe petrophysical properties of facies in the delta lobes. Variograms quantify the spatial correlation of permeability in lithofacies. The lengths of bed-draping shales were estimated from outcrop data using a termination frequency model. The spatial distribution of concretions was modeled with indicator geostatistics.

Flow models integrated bedding geometry, lithofacies, and petrophysical properties in an appropriate structure for reservoir simulation. These models were used to analyze sensitivity of reservoir behavior to different geologic features and to investigate methods for modeling and upscaling interwell-scale heterogeneity. Intrafacies variability of permeability has negligible effects at the sandstone-body scale but significant effects at the bed scale. Shale lengths increase toward the lateral margins and toward the base of the sandstone bodies. Inclined shales reduce upscaled permeability, recovery efficiency, and breakthrough time. Calcite concretions decrease upscaled permeability. An upscaling method based on flow simulation and response-surface models accurately and efficiently represents the effects of geologic heterogeneity and flow rate on a coarse simulation grid.

INTRODUCTION

Production prediction, field development, and economic evaluation rely on quantitative models of reservoir geometry and rock properties. Where the distribution of reservoir and sealing units in the subsurface is complex, naively averaged models cannot adequately predict reservoir performance or uncertainty. Reservoir simulators can predict reservoir behavior in the presence of known geologic heterogeneities, but description and prediction of all scales of geologic variability that may influence subsurface fluid flow is a daunting task. Although small-scale rock-property variations are evident in cores and well logs, and larger scale heterogeneities are detectable by seismic surveys and can be correlated between wells, interwell-scale variations are difficult to quantify in reservoirs. Outcrop analog studies bridge this interwell-scale gap in defining reservoir variability.

Although sequence-stratigraphic and facies models define large-scale reservoir units and describe patterns of small-scale subsurface variability, these models sparsely predict spatial variability of reservoir properties. Engineering models must predict fine- and interwell-scale heterogeneity in reservoirs. Deterministic and stochastic techniques may be used in concert to predict heterogeneity in complex reservoirs (Rossini et al., 1994). Developing and testing models of interwell-scale variability requires quantitative geologic data from demonstrably analogous outcrops to define the geometry, distribution, and magnitude of geologic variations that can affect subsurface fluid flow.

Reservoir simulation studies are time-consuming and expensive because each reservoir is a unique case, consisting of specialized geologic measurement and inference methods, sensitivity analysis, and simulation procedures. Situations that might require such models include high-cost areas (e.g., turbidite reservoirs in the Gulf of Mexico; Lerch et al., 1996), complex reservoirs for which simple descriptions are inadequate (e.g., tide-influenced reservoirs in Venezuela; Ambrose et al., 1995), reservoirs with complex recovery processes (e.g., miscible gas displacements; Hewett and Behrens, 1993), and exceptionally valuable assets (e.g., Prudhoe Bay; Tye et al., 1999). As knowledge of heterogeneity in different depositional environments improves, models become more standardized and easier to use. As computing technology continues to advance, reservoir simulation and associated technologies will be used increasingly often to evaluate alternative reservoir development strategies and to quantify economic uncertainty (Begg et al., 2001). Studies of outcrop analogs help develop efficient, accurate models for reservoir description, simulation, and evaluation.

A particular geologic feature may or may not complicate prediction of reservoir behavior. Some types of geologic variability can be represented adequately using simple averages, whereas predicting effects of other types requires detailed spatial descriptions. Where heterogeneities are complex and occur at multiple scales, it is difficult to discern a priori which features exert the greatest influence on reservoir behavior or to define averaging rules for flow properties. Flow simulations of high-resolution outcrop data quantify effects and

interactions of different types and scales of heterogeneity. Experimental design helps construct efficient, accurate sensitivity studies (Kjønsvik et al., 1992). Identifying the geologic features that have significant effects on reservoir behavior focuses data collection and modeling efforts to improve reservoir description.

Fine-grid, interwell-scale geologic models usually must be upscaled to be feasible for use in fieldwide simulation studies. Geostatistical models and upscaling methods can be tested against data-rich outcrop data sets. In oil and gas reservoirs, engineering parameters such as fluid properties and production rates influence the relative importance of geologic features. For example, the impact of permeability heterogeneity commonly varies as the flow rate or direction varies (Dake, 1978; Durlofsky, 1997). Such interactions between engineering and geologic factors affect sensitivities, performance predictions, and estimates of coarse-grid or upscaled properties. Screening, upscaling, and prediction methods should capture these dependencies.

This chapter describes an outcrop study of a tide-influenced sandstone exposed in central Wyoming. The Frewens Allomember is analogous to lithologically complex reservoirs in the North Sea (Brandsæter et al., 2001), South America (Ambrose et al., 1995), and Southeast Asia (Kurniawan et al., 2001). Outcrop studies of reservoir analogs integrate data from many specialties to (1) establish the sequence-stratigraphic framework and depositional environments of the deposits to identify analogous settings, (2) quantify sedimentologic and petrophysical variations on a hierarchy of depositional strata, (3) determine the burial history and diagenetic overprint, thereby separating depositional and diagenetic controls, (4) identify the most important geologic features defining reservoir heterogeneity, (5) develop models that can be used to predict the distribution of important heterogeneities in reservoirs, and (6) verify that geologic models and upscaling methods correctly characterize fine-, interwell-, and large-scale effects on reservoir behavior.

In the following sections, the regional stratigraphy, sedimentology, and diagenesis of the Frewens sandstone are discussed first. Methods to quantify geologic variability are then addressed. Subsequent sections describe methods to predict heterogeneities in the subsurface, and flow simulations illuminate sensitivities and upscaling. The chapter concludes with a discussion of how these data can be used to improve reservoir models and performance predictions.

GEOLOGIC SETTING

Regional Scale

The Frontier Formation is an Upper Cretaceous (Cenomanian age) clastic wedge that prograded eastward from the Sevier orogenic belt into a foreland basin flooded by the Western Interior Seaway of North America (Figure 1A, B; Barlow and Haun, 1966; Dyman et al., 1994). The Mowry and Cody shales, thick marine mudstones deposited during widespread transgressions, bound the Frontier Formation below and above, respectively (Figure 1C). The Frontier Formation thins eastward from a kilometer-thick fluvial and shoreline succession in western Wyoming. In central Wyoming, it is a few hundred meters–thick succession that is cut by several major unconformities and composed of gradually upward-coarsening, shallow-marine sandstones interbedded with thick marine mudstones (Barlow and Haun, 1966; McGooky et al., 1972). The basal part of this clastic wedge, the lower Belle Fourche Member of the Frontier Formation, contains four unconformity-bounded, upward-coarsening successions (termed Harlan, Willow, Frewens, and Posey Allomembers, Figure 1C), each of which records the progradation of shorelines across the low-gradient floor of the Cretaceous Interior Seaway. Erosion surfaces at the tops of these allomembers placed sealing offshore mudstones directly over the sandstones.

The distal ends of sandstones capping allomembers outcrop on the western edge of the Powder River Basin in central Wyoming (Figure 1A, B; Merewether et al., 1979; Tillman and Merewether, 1994, 1998; Bhattacharya and Willis, 2001). Lower Belle Fourche allomembers were mapped from outcrops southeast of the Bighorn Mountains and hundreds of well logs in the adjacent Powder River Basin (Figure 1D, E). The allomembers have broad lobate shapes, gradational bases with underlying shales, upward-coarsening facies, internal basinward-dipping beds, and basinward-radiating paleocurrents (Bhattacharya and Willis, 2001).

Geometries, lithologies, paleocurrents, and the position in the basin suggest that the lower Belle Fourche allomembers were deposited on lowstand deltas many hundreds of kilometers from highstand shorelines to the west. Erosion surfaces capping allomembers are interpreted to record transgressive ravinement that removed all delta-top facies, leaving only delta-front and prodelta sediments. The lack of distributary channel deposits, flood-plain or tidal-flat mudstones, and coals at the top of deltaic sandstones contrasts with observations of highstand delta systems (Barton, 1994). The thickest parts of successive delta sandstones are laterally offset (Figure 1F), indicating a low accommodation setting. Subtle tectonic warping of the basin floor influenced the site of delta deposition and the extent of ravinement during subsequent transgressions (Bhattacharya and Willis, 2001).

Most of the lower Belle Fourche allomembers (Harlan, Willow, and Posey) contain wave-dominated delta deposits with open-marine styles of bioturbation

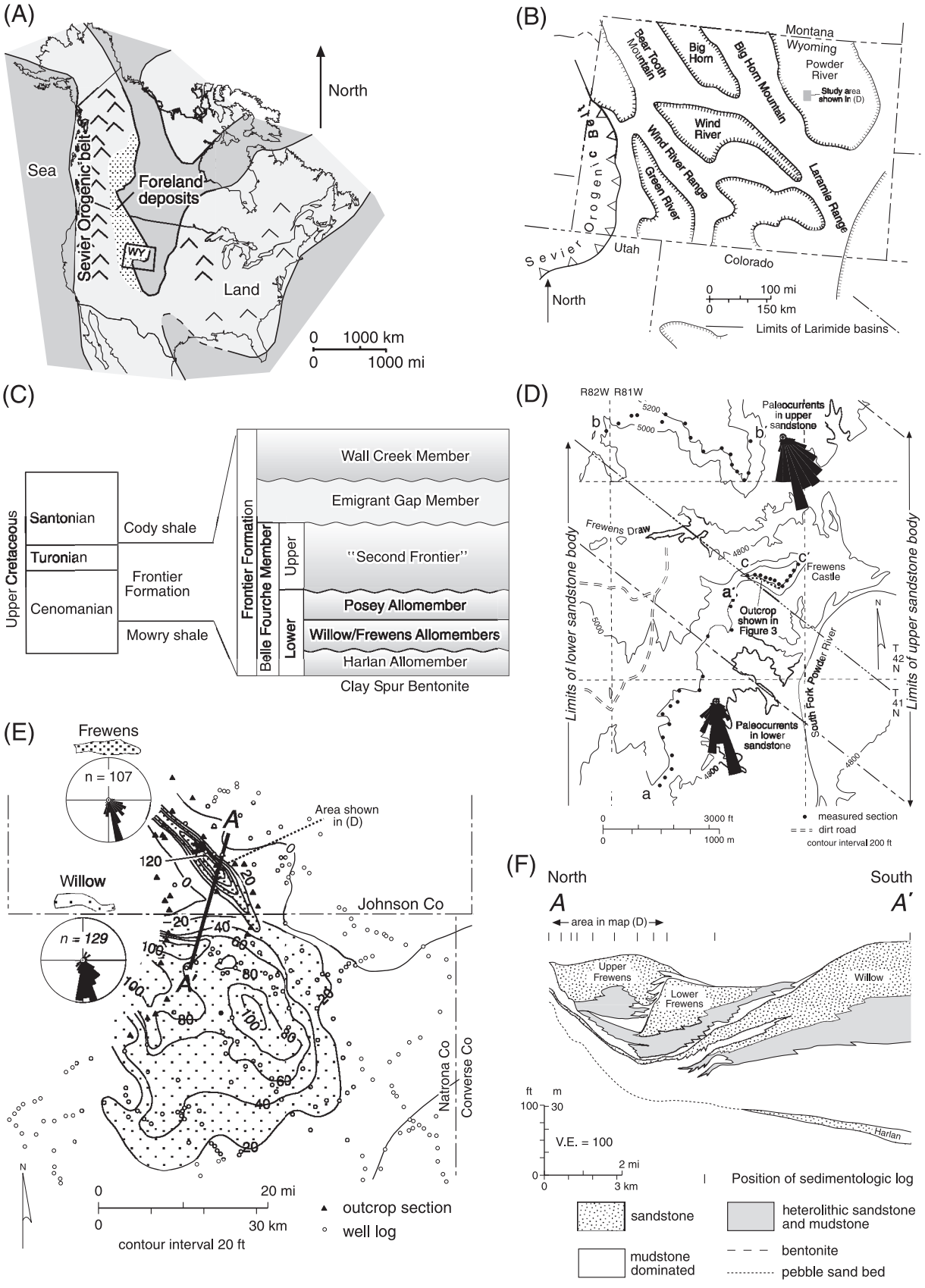
(A)
North
Sea
Sevier Orogenic belt
Foreland deposits
WY
Land
0 1000 km
0 1000 mi
(B)
Montana
Wyoming
Powder River
Study area shown in (D)
Bear Tooth Mountain
Big Horn
Big Horn Mountain
Wind River
Wind River Range
Green River
Laramie Range
Sevier Orogenic Belt
Utah
Colorado
North
0 100 mi
0 150 km
Limits of Larimide basins
(C)
Upper Cretaceous
Santonian
Turonian
Cenomanian
Cody shale
Frontier Formation
Mowry shale
Frontier Formation
Belle Fourche Member
Upper
Lower
Wall Creek Member
Emigrant Gap Member
"Second Frontier"
Posey Allomember
Willow/Frewens Allomembers
Harlan Allomember
Clay Spur Bentonite
(D)
R82W R81W
Paleocurrents in upper sandstone
Frewens Draw
Frewens Castle
Outcrop shown in Figure 3
Paleocurrents in lower sandstone
South Fork Powder River
Limits of lower sandstone body
Limits of upper sandstone body
T 42 N
T 41 N
0 3000 ft
0 1000 m
measured section
dirt road
contour interval 200 ft
(E)
Frewens
n = 107
Area shown in (D)
Willow
n = 129
Johnson Co
Natrona Co
Converse Co
0 20 mi
0 30 km
contour interval 20 ft
outcrop section
well log
(F)
North
South
area in map (D)
Upper Frewens
Lower Frewens
Willow
Harlan
ft m
100 30
V.E. = 100
0 2 mi
0 3 km
Position of sedimentologic log
sandstone
heterolithic sandstone and mudstone
mudstone dominated
bentonite
pebble sand bed

(Bhattacharya and Willis, 2001). These deposits coarsen upward and have gradual lateral facies changes. The deposits of the Frewens Allomember are generally more heterogeneous than the Harlan, Willow, and Posey Allomembers.

The Frewens Allomember is interpreted to be a tide-influenced delta formed in an embayment between the wave-dominated lobes of the Willow Allomember and a tectonic uplift (Figure 1F). The tidal deposits of the Frewens Allomember have pronounced internal heterogeneities related to tidal deposition and postdepositional diagenesis. These tide-influenced delta deposits were the focus of this reservoir analog study.

Depositional Variations in the Frewens Allomember

A 30–50-m-thick succession of tidal deposits comprises the 5-km-wide and at least 20-km-long sandstone bodies of the Frewens Allomember (Figure 1E, F). To the northwest, these deposits were uplifted long after deposition and exposed at the edge of the Bighorn Mountains (Figure 1B). To the southeast, they grade over several kilometers into marine mudstones.

Heterogeneities in the Frewens Allomember occur in a hierarchy of depositional strata. At the largest scale, the allomember contains two upward-coarsening sandstone bodies, each as much as 35 m thick (Figure 1F). Both bodies have gradational bases and erosional contacts with overlying shales. Like the entire Frewens Allomember, the internal sandstone bodies are elongate along a northwest-southeast axis (Figure 1D). Depositional paleoflows are dominantly southeastward along this trend. The ratio of sandstone to mudstone, the grain size of sandstones, and sandstone bed thickness increase upward and toward the axis of each body. The two bodies are laterally juxtaposed; the upper is positioned to the northeast of the lower (Figure 1D, F). The upper body thins along strike and becomes heterolithic (i.e., centimeter-scale interbedded shale and sandstone), where the lower body is thickest and most sandstone rich.

Each body contains beds that are inclined basinward at as much as 5–15° (Figure 2B) and are near horizontal in strike view (Figure 2A). In outcrops exposing dip views, steeply dipping beds in the upper parts of sandstone bodies tangentially decrease in dip to the base of the sandstone body. Bed geometries change along dip over hundreds of meters from thin and gently inclined downdip to progressively thicker and more steeply inclined updip. Finer-grained beds generally have lower dip angles, and they are usually continuous over long distances as nearly horizontal strata along the base of the sandstone body (Figure 2B, C). Steeper, sandier beds downlap onto these finer-grained beds, and the sandier beds are less continuous laterally. Along strike, sandier beds are lens shaped and stack in an offlapping pattern away from axes of the sandstone body (Figure 2A).

The gradual upward-coarsening within bodies is interpreted to reflect conformable deposition during shoreline regression, whereas the eroded tops reflect ravinement during transgression. The general pattern of sandstone-body growth recorded by inclined beds indicates that sediment accreted basinward during progradation rather than by lateral migration of a large-scale bedform. Each sandstone body is interpreted to record progradation of a tide-influenced delta lobe into a narrow embayment (Figure 1F). Deposits are richer in sandstone upward within bodies and toward their axes because of more energetic currents where waters shoaled onto these deltas. Bedding in sandstone bodies records the delta's shape. Steeper-dipping delta-front

Figure 1. Study location and allomember geometry. (A) Paleogeographic map of the Cenomanian Seaway showing location of Wyoming in the developing foreland (Bhattacharya and Willis, 2001). (B) The Frewens Allomember is exposed in the Laramide Powder River Basin in central Wyoming. (C) Age and stratigraphic units in the Frontier Formation of central Wyoming. (D) The Frewens Allomember outcrops in cliffs near Frewens Castle, overlooking the South Fork of the Powder River. The sandstone bodies are elongate along their northwest-southeast–trending axes. Measured sections (dots on map) compiled sedimentologic data and were used to correlate bedding surfaces (Figure 2). Dashed northwest-southeast–trending lines show where the sandy portions of the upper and lower sandstone bodies are more than 5 m thick. (E) Isolith map of two Lower Belle Fourche allomembers shows the lobate shape of the Willow Allomember and elongate shape of the Frewens Allomember. The map was constructed from outcrop sections on the western edge of the Powder River Basin (triangles) and subsurface logs located east of the outcrop belt (unfilled circles). The two sandstone bodies in the Frewens Allomember are not differentiated in this map (simplified from Bhattacharya and Willis, 2001). Paleoflows for both sandstones are skewed south relative to the sandstone body axes. (F) A cross section perpendicular to the axis of the Frewens Allomember shows two laterally offset sandstone bodies, each about 3 km wide. The sandstones overlie the wider Willow Allomember. The Frewens Allomember is deposited in a narrow embayment between a tectonic uplift to the north and the earlier Willow Allomember to the south. This cross section was constructed from outcrop sections projected into plane AA′ (part E). A bentonite bed above this stratigraphic interval was used as the elevation datum (Willis et al., 1999; Bhattacharya and Willis, 2001).

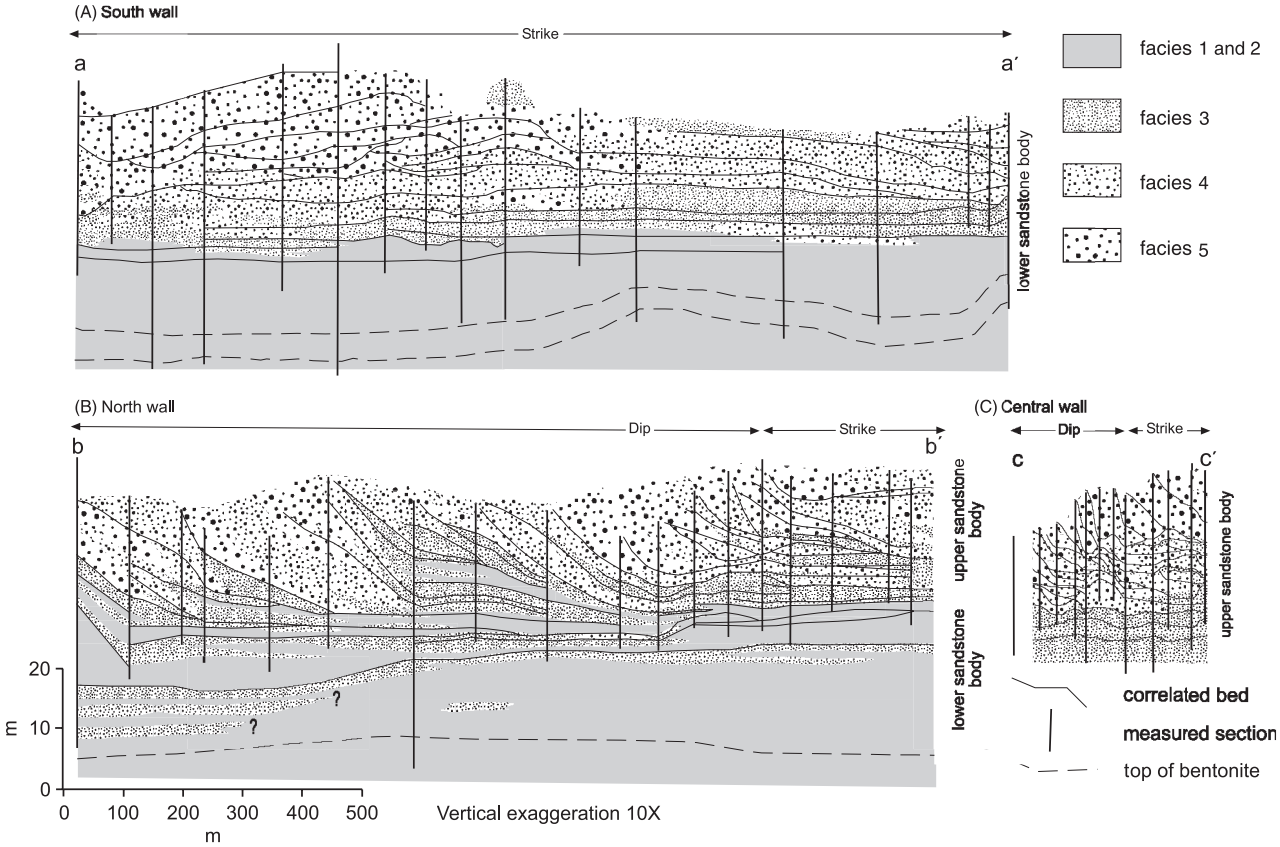

FIGURE 2. Bedding and lithofacies distribution in sandstone bodies. (A) The strike-parallel exposure of the lower sandstone body from cliffs along the South Fork of the Powder River (Figure 1D, aa′) shows lobate bed geometry, with beds offlapping away from the sandstone body axis. Facies have a coarsening-upward trend. (B) A dip-parallel view from the north wall above Frewens Draw (Figure 1D, bb′) shows basinward-shingled bedding. Bed dip decreases downward. (C) The central wall (Frewens Castle) exposes the upper sandstone body in both dip-parallel and strike-parallel views (Figure 1D, cc′; Figure 4; Willis et al., 1999).

beds occur where the delta prograded fastest along its axis, whereas gentler-dipping beds occur in slower-growing areas near the delta margins. These bedding patterns record localized deposition on the delta front, perhaps related to the growth of individual tidal-channel mouth bars.

Individual beds are defined by decimeter- to meter-thick variations between sandier and more heterolithic lithofacies. Episodes of delta progradation that deposited the sandier lithofacies alternated with quiescent periods, when tides reworked delta fronts and deposited the more heterolithic lithofacies. Erosion locally removed shale drapes capping beds, especially in the upper part of sandstone bodies. Thus, shales tend to be less continuous in upper and axial parts of bodies relative to basal and marginal parts.

Lithofacies in beds reflect varying wave and tidal current action during individual depositional events on the delta. Where an inclined bed is traced upward in a sandstone body, deposits generally change through five lithofacies (Figure 3): (1) centimeter-thick interbeds of sandstone and shale recording transport of

FIGURE 3. Lithofacies descriptions. Variations in bed thickness, sedimentary structures, and abundance of fine-scale draping shales are used to divide the deposits into five lithofacies: (1) thinly interbedded, wave- and current-rippled sandstones and mudstones; (2) decimeter-thick cross-sets isolated in lithofacies 1; (3) meter-thick beds of heterolithic cross-sets with abundant evidence of tidal modulation of depositional flows; (4) meter-thick beds of relatively homogeneous, cross-stratified sandstones; and (5) meter-thick cross-sets of homogeneous sandstone. Higher-numbered lithofacies are coarser grained on average and have higher permeability geometric means and coefficients of variation. The net-to-gross of facies 1 is approximately 50%, facies 2 and 3 have net-to-gross greater than 90%, and facies 4 and 5 have net-to-gross near 100%. On the permeability plots, *n* is the number of samples, gm is the geometric mean, *m* is the arithmetic mean, sd is the standard deviation, sk is skewness, and cv is the coefficient of variation (Willis et al., 1999).

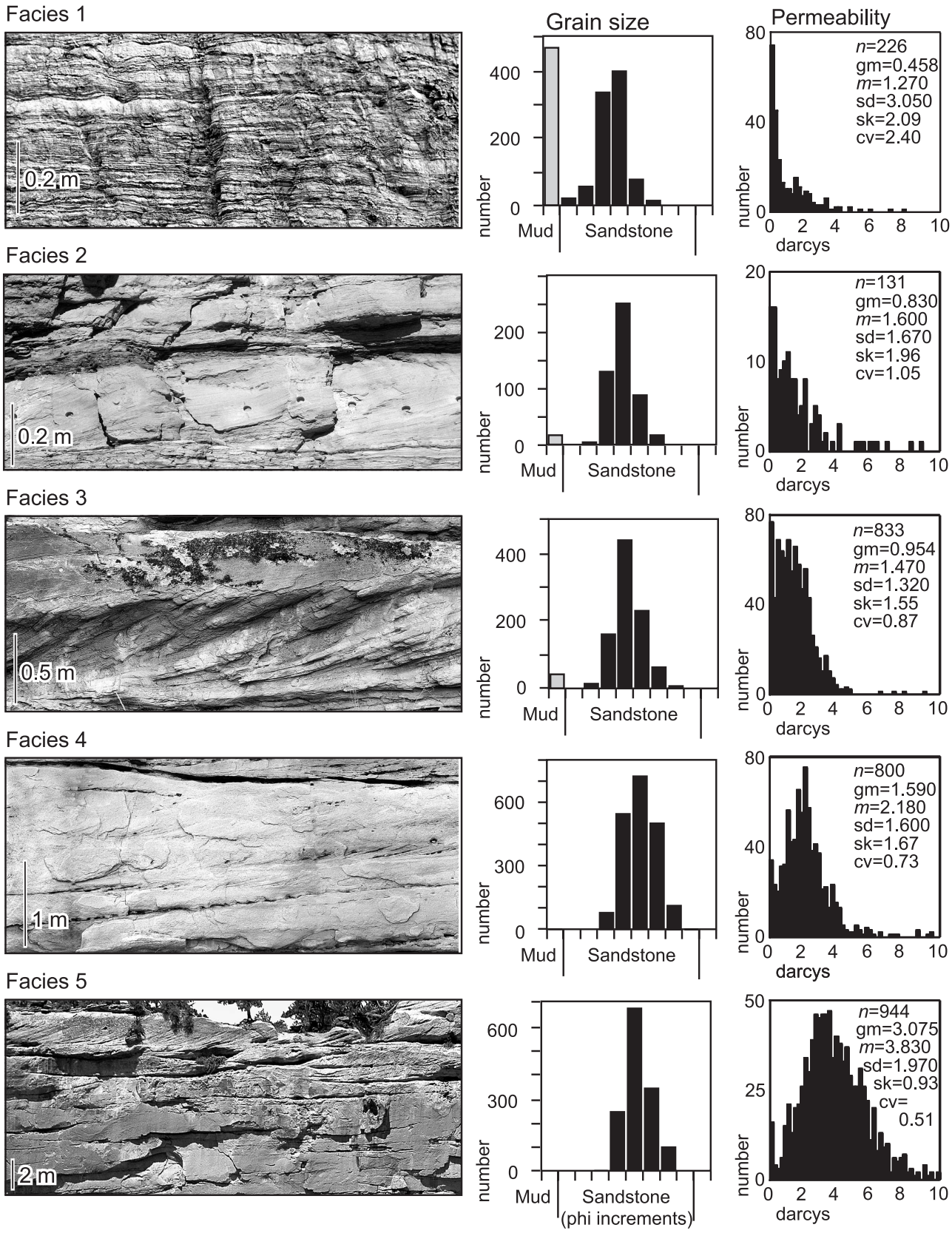
Facies 1
Grain size
Permeability
0.2 m
400
200
0
number
Mud
Sandstone
80
40
0
n=226
gm=0.458
m=1.270
sd=3.050
sk=2.09
cv=2.40
0 2 4 6 8 10
darcys
Facies 2
0.2 m
200
100
0
n=131
gm=0.830
m=1.600
sd=1.670
sk=1.96
cv=1.05
20
10
Facies 3
0.5 m
n=833
gm=0.954
m=1.470
sd=1.320
sk=1.55
cv=0.87
Facies 4
1 m
600
300
n=800
gm=1.590
m=2.180
sd=1.600
sk=1.67
cv=0.73
Facies 5
2 m
50
25
n=944
gm=3.075
m=3.830
sd=1.970
sk=0.93
cv=
0.51
Sandstone
(phi increments)

rippled sandstone sheets to the distal end of the sandstone body; (2) decimeter-thick sandstones recording sand transported in starved dune fields; (3) heterolithic cross-strata recording the aggradation of dunes that were frequently reworked by tidal currents; (4) sandy, decimeters-thick cross-strata formed by dunes that migrated more consistently basinward; and (5) meters-thick sandy cross-strata formed on larger-scale dunes or steep-faced, basinward-migrating bars (Willis et al., 1999). The upward change in lithofacies reflects increasing sediment supply and stronger ebb-oriented currents higher on the delta front.

Although beds generally coarsen and become less heterolithic when traced upward along depositional dip in the sandstone body, at any specific location most beds fine upward. High in the sandstone bodies, beds generally have erosional bases and contain several meters of facies 5, abruptly overlain by approximately a centimeter of facies 1 or the basal erosion surface and mud-chip lag of the overlying bed. Central parts of beds are composed of meters of facies 4 that grade upward into a similarly thick interval of facies 1–3. The distal toes of beds are composed of decimeters to meters of facies 1–3 that grade downdip (over hundreds of meters to a kilometer) into approximately 1 dm of facies 2 isolated by a thicker layer of facies 1.

Composition and Diagenesis of the Frewens Allomember

The Frewens sandstones are lithic arkoses with an average composition of $Q_{42}F_{31}R_{27}$ (Dutton et al., 2000); orthoclase and plagioclase feldspars are approximately equally abundant. Chert is the most abundant rock fragment; volcanic, metamorphic, and plutonic rock fragments also are present. The lower sandstone body is slightly richer in plagioclase and volcanic rock fragments than the upper sandstone body. Both sandstones contain volcanic quartz grains. Diagenesis in most Frewens sandstones has been relatively minor, except for precipitation of iron-bearing calcite cement localized in large, tabular concretions (Dutton et al., 2000). Clay, probably mixed-layer illite/smectite, rims some detrital grains. There are small overgrowths on some quartz grains, but the average volume of quartz cement is only 1%. Kaolinite (less than 2%) occurs in both primary and secondary pores.

Calcite in many concretions has partly dissolved, and hematite has precipitated in the resulting pores. The hematite stains the concretions with a reddish color, so that they can be distinguished from uncemented sandstones (Figure 4A, E). Petrographic and isotopic data suggest calcite cement in the Frewens sandstone precipitated near the maximum burial depth of the sandstones (1.5 km) from evolved meteoric water or mixed meteoric and marine pore waters (the $\delta^{18}O$ composition of the calcite ranges from −9.3 to −12.4‰ Peedee belemnite [PDB], and the $\delta^{13}C$ composition ranges from +0.1 to −14.2‰ PDB; Dutton et al., 2000). The $\delta^{13}C$ composition indicates that the source of carbon was mostly biogenic carbonate, with a contribution of ^{13}C-depleted carbon derived from oxidation or decarboxylation of organic matter. No fossil fragments or molds of dissolved fossils and very few trace fossils occur in the Frewens sandstone. This indicates that little internal biogenic carbonate was present. Instead, shell-bearing marine shales above the upper Frewens sandstone are interpreted to be the source of the biogenic carbonate (Dutton et al., 2000).

Calcite concretions occur in both the upper and lower Frewens sandstone bodies, but they are more abundant in the upper body, particularly in the high-permeability, cross-stratified facies in the upper part of the sandstone body (Figure 4A, E). A greater concentration of cement in the most porous and permeable sandstones was observed on a larger scale as well. Calcite cement is more abundant where successive beds become thicker, sandier, and more steeply inclined along a dip cross section. Similarly, calcite cement is more abundant in the sand-rich deposits at the axes of the sandstone bodies than in the finer-grained deposits along their margins.

QUANTITATIVE DESCRIPTION OF HETEROGENEITIES

Qualitative descriptions of depositional and diagenetic heterogeneity in the Frewens Allomember indicate the style of interwell-scale facies variations and bedding geometry, but they do not provide data to predict heterogeneities in analogous reservoirs. Outcrops provide data for features and scales that cannot be observed in subsurface reservoirs. Quantitative data must be obtained from well-exposed outcrops where the stratigraphic setting can be inferred, strata can be delineated, lithologies can be mapped, and rock properties can be measured. Methods to compile quantitative data for the geologic heterogeneities in the Frewens Allomember are described below.

The Frewens Allomember Database

Sandstones of the Frewens Allomember are best exposed in and adjacent to Frewens Castle, along the South Fork of the Powder River in central Wyoming (Figure 1D). The lower sandstone body outcrops in a 3-km strike section that exposes its axis and northern margin. The upper sandstone body outcrops in a kilometer-long

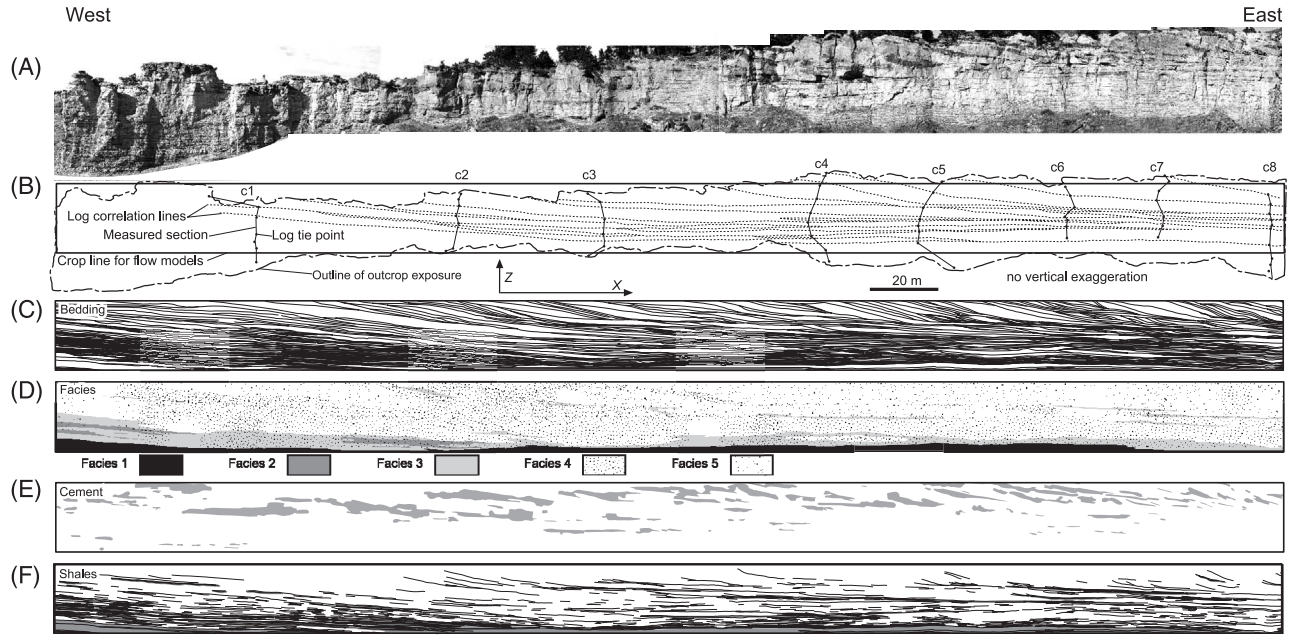

FIGURE 4. Detailed bedding and lithofacies distribution of the dip-parallel wall of Frewens Castle (Figures 1D, 2C). Different geologic features were recorded on separate overlays for statistical and reservoir-simulation studies. (A) Photomosaics were prepared by digitally splicing and editing to reduce perspective distortions. The deposit coarsens upward to a capping erosion surface that is overlain by shale. (B) The database combined sedimentologic logs, bedding diagrams, and other data to produce gridded models. Areas where data were cropped or extrapolated are shown by the limits of outcrop exposure and the flow model boundaries. The coordinate systems of bedding diagrams and positions of rock property samples on vertical logs (labeled c1–c8) were rectified using beds correlated between adjacent logs and log tie points on bedding diagrams. (C) The bedding diagram includes 697 beds. (D) The deposits are divided into five lithofacies with different internal heterogeneity and permeability distribution. Facies labeled by higher numbers and shown by coarser stippling are generally coarser grained, less heterolithic, and more permeable (Figure 3). (E) Calcite concretions were mapped based on a reddish stain (part A), permeability measurements, and field observations. (F) Thin shale drapes on bed boundaries were mapped using photomosaics and field observations. Gray-shaded areas are shale-rich zones (Willis and White, 2000).

dip section along its axis and in smaller adjacent outcrops exposing its margins. Frewens Castle exposes both dip and strike sections of the upper sandstone body. Photomosaics of these outcrops were constructed by digitally splicing a succession of photographs taken on medium-format film from a helicopter (e.g., Figure 4A). The photographs were corrected using an image-processing program and survey data to remove as much perspective distortion as possible.

Photomosaics were used to map bedding, facies, shale drapes, and calcite concretions on separate transparent overlays (Figure 4). Sedimentologic logs measured about every hundred meters along these outcrops (Figures 1D, 4B) initially delineated lithofacies, and positions on these logs were tied to outcrop photomosaics. Permeabilities were measured along many of these sedimentologic logs with a probe permeameter (Goggin, 1993; Barton, 1994; Willis, 1998). The database records grain size, facies type, mean bed thickness, and permeability measurements made every 0.2 m along each vertical log. The transparent overlays were digitized into different layers of a standard drafting program to align bedding, facies, and shale maps and to specify log tie points (Willis and White, 2000).

Additional permeability measurements record fine-scale horizontal variability in each lithofacies type. Horizontal traverses measured permeability every 0.2 m along representative beds of each lithofacies over distances of 30–100 m. Short vertical logs and logs following inclined strata in these lithofacies were tied to these long horizontal traverses. Detailed photomosaics of smaller-scale strata, shales, and concretions in lithofacies also were produced. These finer scale studies focused on heterolithic cross-sets of facies 3 (Willis and White, 2000; White et al., 2001). Internal heterogeneity in this lithofacies was expected to have a greater impact on flow predictions than in lithofacies 4 and 5, which are more homogeneous. Lithofacies 1 and 2 are unlikely to be major flow conduits because of their lower permeability and continuity.

Cliffs, positions of logs, and sites of the more detailed lithofacies studies were surveyed using a theodolite with laser range finder (a ''total station'') to position them in a consistent coordinate system. The

final database had a highly structured format (White and Barton, 1999; Willis and White, 2000). Bedding diagrams (Figure 4C) are specified as a set of line segments defined by irregularly spaced (x,z) points honoring these rules: (1) bedding surfaces end only at the diagram boundaries or at another bedding surface, (2) bedding surfaces cannot cross, and (3) no bedding surface can circle back on itself in the horizontal direction. Line segments define bed-draping shales, with each shale precisely overlying a bed boundary in the bedding diagram. Closed polygons that entirely cover the bedding diagram describe the distribution of lithofacies (Figure 4D). Concretions also are mapped as closed polygons (Figure 4E). Small differences between thicknesses recorded by vertical logs and the bedding diagrams are resolved by linearly interpolating log data between tie points to the bedding diagram.

The large-scale outcrop maps of lithofacies (generally hundreds of meters in horizontal extent) average out smaller-scale variations in individual beds. Generalized mapping of lithofacies is required because it is impossible to record every facies transition where depositional beds are very thin. This convention eliminates variation in map resolution with local changes in outcrop quality. However, thin, laterally continuous shales often have important influences on flow behavior. For this reason, these shales were included in the database by mapping them separately from the facies polygons as line segments lying on bedding surfaces (Figure 4F).

Several two-dimensional ground-penetrating radar (GPR) transects over the upper Frewens sandstone body were collected to test the ability of this method to image heterogeneities observed in the outcrop cliffs (e.g., Figure 5). GPR data with a nominal frequency of 100 MHz delineated beds and sets of beds in the upper sandy part of the deposit but was unable to resolve bedding in the more heterolithic facies lower in the deposit (Figure 5D). At its best, the resolution of this GPR record (several decimeters) is coarser than many of the features examined in outcrop studies (particularly bed-draping shales, Figure 5C). Even where the deposits were quite sandy, the depth of penetration seldom exceeded 10 m (about one-third of the sandstone-body thickness). GPR traverses across exposed bedding planes kilometers away from the outcrops were more difficult to interpret than those adjacent to outcrops. Many bedding planes in areas adjacent to the outcrops are covered by loamy soils that block GPR penetration into the underlying sandstone body. High-resolution seismic would have greater depth of penetration than GPR (more than 100 m at 1 kHz), but resolution is poorer (approximately 0.5 m; Nissen et al., 1999). This resolution is adequate to delineate sandstone-body dimensions, but it cannot define the distribution of smaller-scale heterogeneities. Although geophysical methods can help establish a three-dimensional framework to aid translation of outcrop data into three dimensions (McMechan et al., 1997; Corbeanu et al., 2001), these methods complement rather than replace detailed outcrop studies to define interwell-scale heterogeneities.

This database was the foundation of the quantitative outcrop study. It was used to

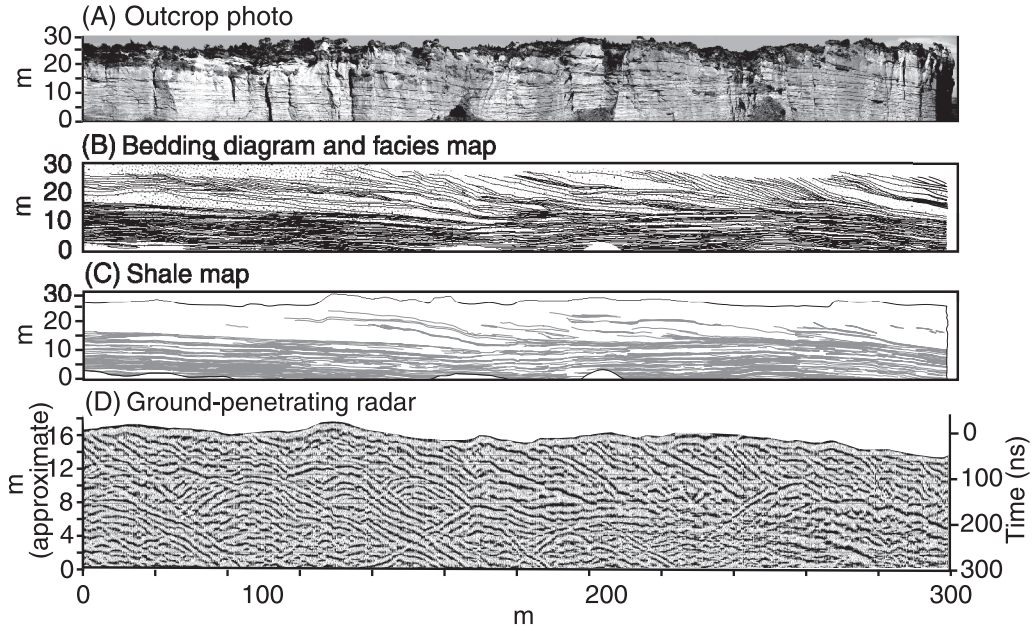

Figure 5. Ground-penetrating radar (GPR) traverse measured about 100 m behind a dip-parallel outcrop of the upper Frewens sandstone body. (A–C) Heterogeneities observed in outcrop can be compared with (D) variations in the GPR record. The radar record was collected with a 1000-v PulseEKKO transmitter and 100 MHz antennas. Larger-scale bedding trends in sandier deposits located in the upper 5–8 m of the outcrop are imaged well by GPR, but bedding in heterolithic deposits observed lower in the outcrop are poorly imaged. High-angle hyperbolic reflectors dominating the lower part of the record show the location of vertical joints passing through the outcrop.

(1) define large-scale vertical trends in each sandstone body, (2) construct geostatistical models of permeability variations across the outcrop exposures, (3) estimate the length distribution of shale beds, (4) predict the distribution of calcite concretions, and (5) construct reservoir simulation models. These investigations are discussed in the following sections.

Permeability Variations in Sandstone Bodies

The lithofacies based on sedimentologic characteristics also group rocks in terms of their fluid-transport properties. The permeabilities of lithofacies commonly vary by several orders of magnitude, whereas porosities generally vary only a few percent. Higher-numbered lithofacies (i.e., facies 4 and 5) are generally coarser grained, more permeable, and thicker bedded (Figure 3). The more heterolithic lithofacies (facies 1–3) have lower geometric mean permeability and greater coefficients of variation than the more homogeneous lithofacies. The permeability distributions of lower-numbered lithofacies are positively skewed, whereas permeability distributions for facies 4 and 5 are approximately symmetric.

Vertical rock-property trends in sandstone bodies were quantified with datum-aligned averages of all logs measured in each of the two Frewens sandstone bodies (Figure 6). Grain size and the amount of thick-bedded, homogeneous lithofacies increase upward in each body. In the lower body, mean permeability also increases upward, whereas in the upper body, permeability decreases upward. Calcite concretions concentrated near the top of the upper sandstone body (Figure 4E) cause this difference in permeability trends. To separate permeability variations caused by depositional processes from those caused by diagenetic processes, rock-property data from the lower, relatively uncemented sandstone body were used to characterize variations in individual lithofacies.

Semivariograms describing permeability variations in each lithofacies were computed using normal-score transformed permeability data from vertical and horizontal permeability logs (Deutsch and Journel, 1998). Heterolithic cross-sets have systematic lateral permeability variations spanning meters to tens of meters; this reflects the lateral variation from coarser-grained sediments deposited in the lee of actively growing dunes to finer-grained sediments deposited when dunes paused and troughs filled (facies 3 semivariogram, Figure 7A). In more homogeneous cross-stratified lithofacies, spatial correlation of permeability was not as significant (facies 5 semivariogram, Figure 7B). These variograms were used to krige or simulate permeability values across the broader outcrop lithofacies maps. These spatial models of permeability will be discussed in the section on flow modeling below.

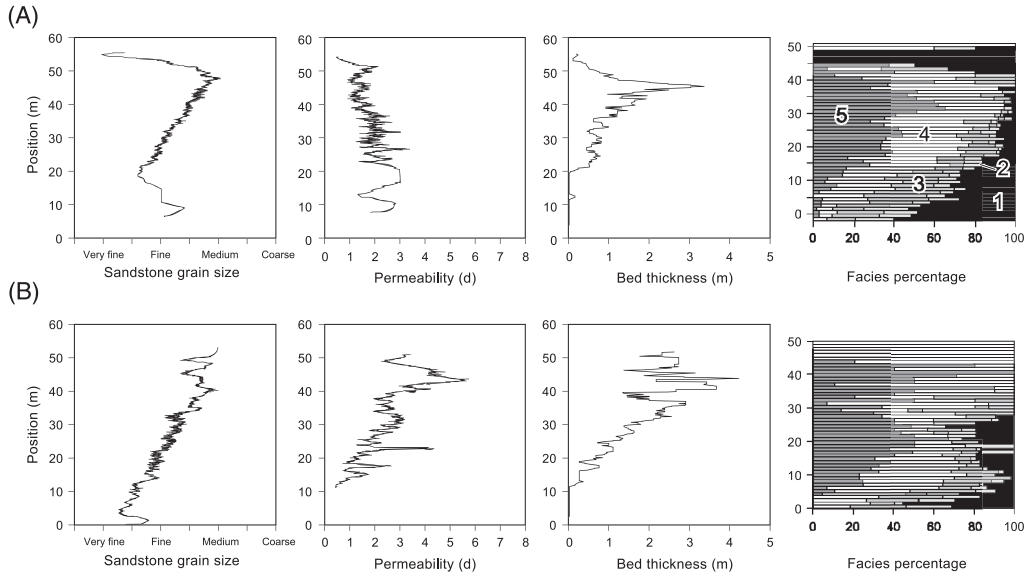

FIGURE 6. Vertical property trends for the Frewens Allomember sandstone bodies. The trends were computed by averaging all measured sections for each sandstone body (Figure 1D). (A) The upper sandstone (spanned by 20 measured sections) coarsens and thickens upward, and higher-numbered facies are more abundant higher in the sandstone body. The permeability decreases because of calcite concretions that are abundant near the top of the upper sandstone body (Figure 4A, E). (B) The lower sandstone body (spanned by 16 measured sections) has consistent trends of upward-increasing grain size, permeability, bed thickness, and facies quality (Willis et al., 1999).

Shale Length Distributions

Upscaled vertical permeability (Prats, 1972; Begg and King, 1985; Desbarats, 1987), upscaled horizontal permeability (Narayanan, 1999), and recovery behavior (Jackson and Muggeridge, 2000; Willis and White, 2000) are affected by shale locations and properties. Modelers have used distributions tabulated directly from outcrop data (Haldorsen and Lake, 1984), indicator geostatistics (Desbarats, 1987), and methods to correct

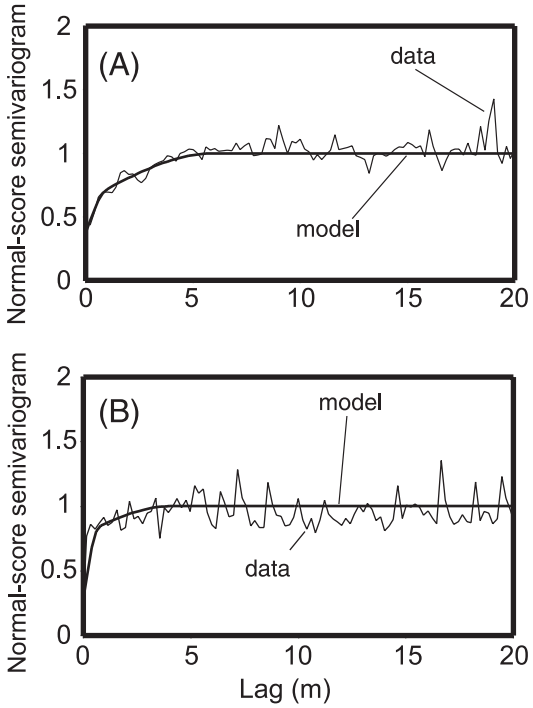

FIGURE 7. Horizontal semivariograms of permeability. Semivariograms are for the normal-score transform of permeability. (A) The semivariogram for facies 3 has correlation to more than 5 m, reflecting active and abandonment phases of dune deposition. (B) Facies 5 has little correlation beyond 2 m, reflecting greater uniformity in depositional conditions compared to facies 3. Facies 5 has a larger nugget effect than facies 3, which indicates lesser spatial correlation of facies 5. Semivariograms also were computed for the vertical direction and other facies (Willis and White, 2000).

observed length distributions for bias in sampling and dimensionality (Geehan and Underwood, 1993; Visser and Chessa, 2000).

More than 6000 shales longer than 1 m were mapped on 14 outcrop exposures of the Frewens Allomember, in both dip- and strike-oriented cliffs and in axial and marginal portions of the upper and lower sandstone bodies (White and Willis, 2000). The shales are shorter at the sandstone-body axis than at the margins (Figure 8). The shales also are shorter higher in the sandstone body. The decreased length of shales probably reflects higher depositional energy and, consequently, less deposition and preservation of shales in these areas. At the sandstone-body margins, many shales extend beyond outcrop boundaries (Figure 8B). Geehan and Underwood (1993) computed a ''typical'' length for the shales extending beyond the bounds of outcrop exposures. Visser and Chessa (2000) estimated the complete distribution for partially observed shales in rectangular sample windows. However, outcrop shapes often are irregular, and this is certainly true for most of the Frewens sandstone exposures (Figures 4, 8). Restricting the analysis to an inscribed rectangle decreases the data set size, motivating the termination frequency model. The termination frequency t is the number of shale terminations observed in the outcrop divided by the total length of shale observed,

$$t = \frac{\sum_{i=1}^{N} n_{ti}}{\sum_{i=1}^{N} \ell_i},$$

where N is the total number of shales observed, n_{ti} is the number of terminations exposed for the ith shale, and ℓ_i is the exposed or observed length of the ith shale. The termination frequency is unbiased regardless of outcrop shape, and for any length distribution, $\bar{\ell} = \frac{2}{t}$ is an unbiased estimate of the mean length (White and Willis, 2000).

Termination frequency models for length distributions are compared with the observed distributions in Figure 9. The observed distributions have been approximately debiased (Geehan and Underwood, 1993). The model distributions are not regression fits but are statistical models with parameters computed directly from observations. These models are composite length distributions, the sum of two termination-frequency models determined by Bayes' rule (White and Willis, 2000). The observed and modeled length distributions for the axial location (Figure 9A) are similar because the average shale length is much less than the outcrop length; the model mean is 16% larger than the observed mean. In contrast, the computed distribution for the outcrop exposure at the sandstone-body margin (Figure 9B) contains many more long shales than were

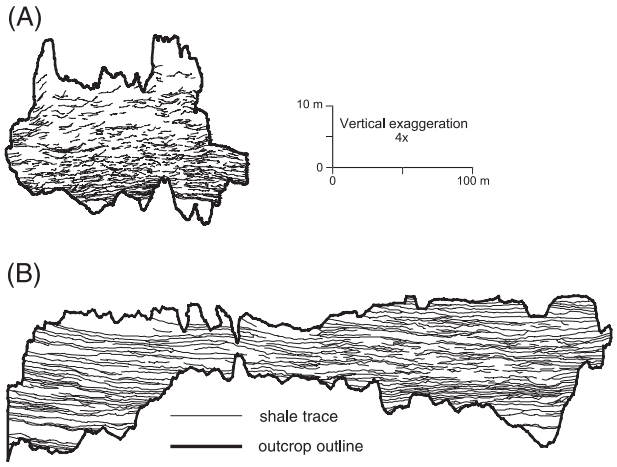

FIGURE 8. Shale maps. (A) Near the axis of the lower sandstone body (point a in Figure 1D), shales are relatively short, and few extend beyond the limits of exposure. (B) Toward the margin (point a′ in Figure 1D) of the lower sandstone body, the shales are much longer, and many extend beyond the outcrop limits (White and Willis, 2000).

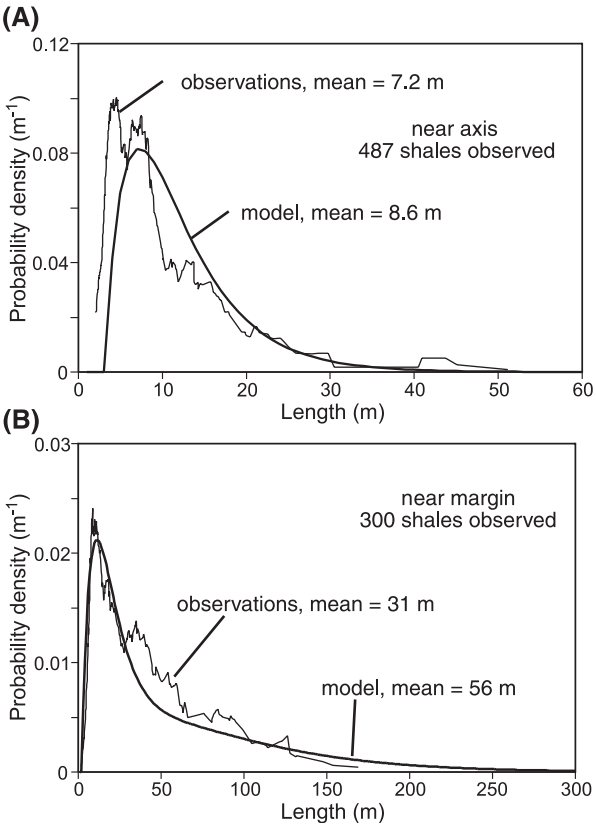

FIGURE 9. Histograms of shale length. The length scales are different for the two histograms. (A) Near the axis, the shales are relatively short, and the model predicts few shales longer than those observed because few shales extend beyond the outcrop (Figure 8A). (B) Near the margin, the model predicts longer shales compared with the observations because many shales extend beyond the outcrop limits (Figure 8B). Shale lengths generally increase toward the sandstone-body margins (White and Willis, 2000).

observed, and the model mean is 45% greater than the observed mean. The large difference between observed and modeled distributions at the margin is expected because the termination frequency model corrects for finite outcrop length, and this correction is significant when the outcrop is not long compared to the mean shale length (White and Willis, 2000). The increase in the estimated proportion of long shales by the model compared with observations is likely to be important in analogous reservoirs: the longest shales have the greatest effects on flow.

The termination frequency and, thus, the mean length and length distribution vary along strike (Figures 8, 9) and vertically (Figure 10). The inferred mean length at the margin is 6.5 times greater than at the axis. No trend was observed along dip. The termination frequency is low near the bottom of the outcrop, reflecting the greater deposition and preservation of shales in deeper water at the base of the delta. The termination frequency is correlated vertically, reflecting cyclic variation in sediment supply, erosion, or locus of deposition. These variations in shale distribution imply that upscaled properties vary throughout the reservoir. This variability should be considered in reservoir models.

The effects of shale depend upon the number of shales as well as their location (Begg and King, 1985). Further, the effects will be significantly different if shales are inclined and especially if shales converge, creating poorly connected compartments (Jackson and Muggeridge, 2000). These effects were observed in the Frewens sandstone (Narayanan, 1999; Willis and White, 2000; White et al., 2001).

Calcite Concretion Distribution

Nodular calcite concretions like those observed in the Frewens sandstone can be detected in cores or geophysical logs (particularly density and neutron logs; Walderhaug et al., 1989; Worden and Matray, 1998), and their abundance and vertical distribution can be quantified from these data. Predicting the lateral dimensions and distribution of calcite concretions in the subsurface is more difficult. This motivated additional calcite concretion statistical description and modeling.

Cement distribution was quantified for a 362-m-long dip-parallel outcrop wall (Figure 4) and an adjacent 216-m-long strike-parallel wall of the upper Frewens sandstone. Median dimensions of the concretions are 0.6 m thick (T), 4.2 m long (L), and 5.3 m wide (W) (Dutton et al., 2000). The median aspect ratio (T/L) of the concretions is 0.11. Concretions comprise

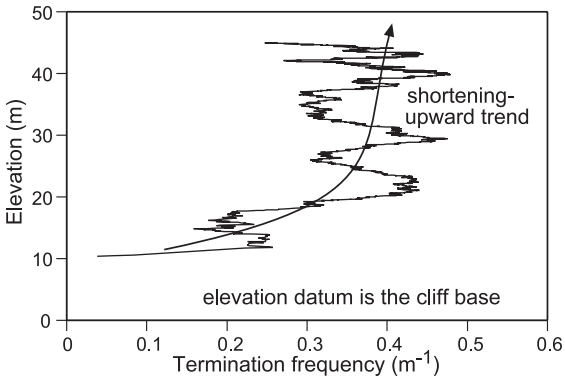

FIGURE 10. Vertical trend in termination frequency. This trend was computed using the strike-parallel face adjacent to the dip face shown in Figure 4 (Figures 1D, 2C). Termination frequency increases upward in the sandstone body (shale length decreases upward). In addition to the overall upward-increasing trend, termination frequency oscillates with a wavelength of approximately 10 m, perhaps reflecting cyclic deposition on the prograding delta (White and Willis, 2000).

12% of the area of the dip-parallel outcrop wall (Figure 4A, E). A horizontal profile of the outcrop (measuring the fraction of the thickness of the upper Frewens sandstone cemented by calcite) has no distinct trend, whereas a vertical profile of the cemented fraction increases toward the top of the outcrop (Figure 11). The average spacing of concretion centers is approximately 1 per 70 m^2 of outcrop face, and their position in the outcrop can be approximated by a Poisson-distributed random variable (Dutton et al., 2002). The upward-increasing trend in cemented fraction (Figure 11) is caused by the upward increase in the size of the concretions. Concretions in the lower 10 m of the dip-parallel outcrop wall have an average area of 1.6 m^2, whereas those in the upper part of the outcrop average 7.7 m^2.

A geostatistical simulation method was developed to distribute concretions in subsurface reservoirs (Dutton et al., 2002). Indicator semivariograms quantify vertical and horizontal correlation of the concretion distribution in the Frewens sandstone. In this calculation, concretion occurrence was modeled using an indicator variable with a value of 1 if calcite cement is significant at a given location and 0 if not significant. The horizontal semivariogram has a range of about 30 m, and the vertical semivariogram has a range of about 2.5 m (Figure 12). These variogram ranges correspond approximately to the size of the largest concretions in the Frewens sandstone (Dutton et al., 2002). The non-

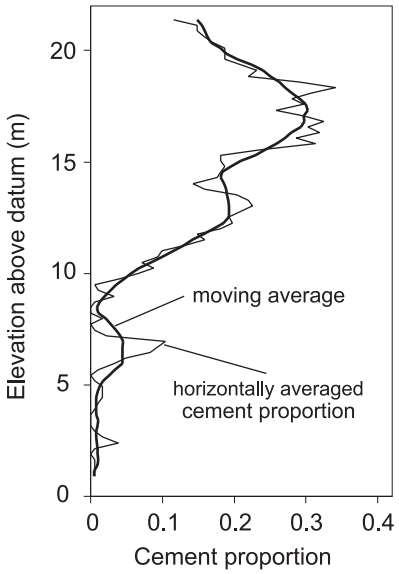

FIGURE 11. Vertical trend in concretion fraction. The proportion of concretions (relative to total area) was averaged at each elevation throughout the sandstone body. The concretion fraction increases upward. This profile was computed using data from the outcrop exposure shown in Figure 4. No lateral trend was observed (Dutton et al., 2002).

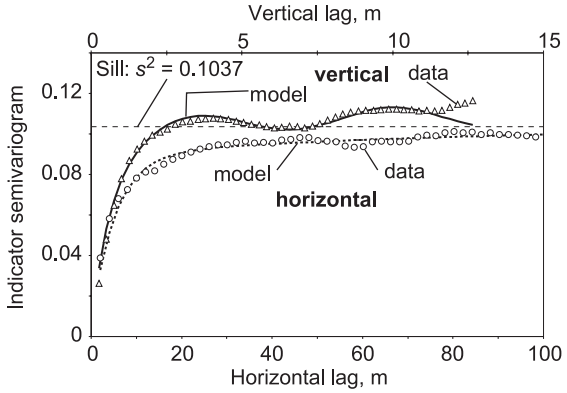

FIGURE 12. Horizontal and vertical semivariograms for the concretion indicator. The observations were computed using a regularly gridded array of concretion indicators (1 for concretions, 0 for no apparent calcite cement; Figure 13A). The horizontal and vertical ranges are approximately 30 and 2.5 m, respectively. The vertical lag is plotted on the axis at the top of the figure (Dutton et al., 2002).

stationary indicator variogram was transformed to the variogram for the related Gaussian variable, and the trend (Figure 11) was incorporated via a proportion curve (Matheron et al., 1987).

Sequential Gaussian simulation with truncation created images with statistically correct correlation and trends and honoring conditioning data (Matheron et al., 1987; Deutsch and Journel, 1998). The conditionally simulated images were postprocessed with simulated annealing (Deutsch and Journel, 1998) and multipoint statistical simulation (Caers et al., 2000) to improve conformance to the observed variogram and image texture. The reference image from the outcrop face (Figure 13A) and a conditional geostatistical simulation (Figure 13B) share many features: the overall proportion of concretions is the same, the vertical trend in cemented fraction is the same, and the average angle of inclination of the concretions is similar. Simulated annealing ensures that the variograms are similar as well. Suites of flow simulations demonstrated that the geostatistical models accurately reproduce the effects of the concretions on fluid flow (Dutton et al., 2002).

GEOLOGIC HETEROGENEITIES AND FLOW OF FLUIDS

Heterogeneities in the Frewens sandstone (discussed above) affect the flow of hydrocarbons and displacing fluids. To understand these effects, flow must be simulated for a range of feasible models. The suite of flow models can be used for sensitivity analysis,

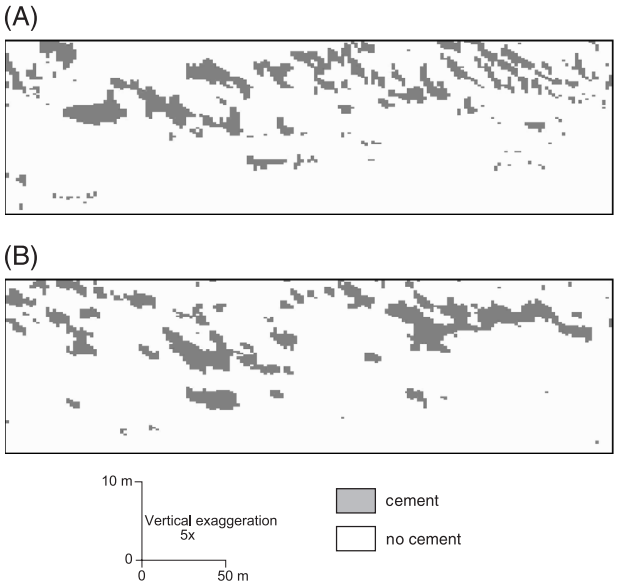

FIGURE 13. Concretion images. (A) The observed concretion map (Figure 4E) was discretized onto a regular rectangular grid. (B) A conditional geostatistical simulated image was prepared using truncated sequential Gaussian simulation, simulated annealing, and multipoint statistics. The simulated image reproduces the smoothed trend (Figure 11), variogram (Figure 12) and inclination of concretions in the reference image. The reference and simulated images (A and B) match at the left and right ends where the simulation was conditioned (Dutton et al., 2002).

testing of geologic models, and upscaling. The flow models used in this study were much more detailed than typical field-scale models. In this study, blocks were about a decimeter thick and 2 m long, whereas blocks in field-scale models are often meters thick and a hundred meters or more in horizontal extent. To incorporate the effects of fine-scale features in field-scale models, the fine-scale models must be upscaled.

Commercial reservoir simulation programs (Schlumberger Technology, 1997; Computer Modeling Group, 1999) were used to examine the flow behavior of models based on the Frewens Allomember. The cornerpoint simulation grid conforms to observed bedding (Willis and White, 2000). The simulation grid (Figure 14A) of the sandstone body in this study retains all the features shown in the high-resolution bedding diagram (Figure 4) with 713 layers and 181 x-direction grid blocks. There are more simulation layers than geologic layers; the vertical refinement improves resolution of lithofacies variations and flow phenomena. The models are two-dimensional; there is no variability or flow in the third dimension. Of the 130,000 total grid blocks, only 13,000 were active. The remaining 117,000 were void grid blocks used to represent areas in layers where beds have terminated. Void grid blocks require few computational resources compared to active grid blocks. Permeability and porosity were assigned based on outcrop measurements with a probe permeameter (Willis and White, 2000) and thin-section point counts (Dutton et al., 2000). Water was injected across the full vertical interval at the left end of the model, and oil and water were produced from the full vertical interval at the right. The simulator well models assigned uniform potential (Dake, 1978) at each end of the flow model. The displacement velocity $\nu = \frac{q_{\text{wir}}}{A\phi}$ was 0.3 m/day; q_{wir} is the water injection rate at bottomhole conditions, A is the cross-sectional area of flow, and ϕ is the porosity. The upper and lower edges of the model are impermeable. Water-wet relative permeability curves were used to model the dependence of oil and water permeability on water saturation (Honarpour et al., 1982). Capillary pressure is very low for such high-permeability sandstones.

Effects of geologic heterogeneities in a 25-m-thick sandstone are illustrated by adding different features cumulatively to successive flow simulation models. The first example is a displacement of oil by water through a grid with uniform single-phase permeability defined by the geometric mean of all permeability measurements (Figure 15A). In the absence of permeability contrasts and other heterogeneity, water sinks to the bottom of the cross section because it is denser than oil. The saturation distribution reflects the interaction of gravity and viscous forces; gravity segregation decreases as flow rate increases.

Varying permeability by lithofacies (Figure 14C) draws the water upward into the high-permeability lithofacies near the top of the sandstone body (cf. Figure 15A, B). Viscous force gradients caused by the rock heterogeneity lift the advancing water in opposition to gravity segregation. Upscaled permeabilities were computed by the pressure-solver method with no-flux lateral boundary conditions (Desbarats, 1987). The upscaled permeability is higher if facies-specific permeabilities (Figure 14C) are used instead of the global geometric mean (820 md for the global geometric mean versus 1700 md if permeability is assigned using facies-specific means; Willis and White, 2000). The global geometric mean underestimates permeability because of the high lateral continuity of the high-permeability strata in the top of the sandstone body; this is the expected result for horizontal permeability (Li et al., 1999).

If intrafacies permeability variations are geostatistically simulated using the facies-specific semivariograms (Figure 14D), the displacement front is slightly more dispersed compared with the models using lithofacies-specific geometric means (cf. Figure 15B, C). Mixing caused by small-scale permeability fluctuations has little effect because the intrafacies permeability-correlation ranges are short compared to the dimensions of the lithofacies polygons (Figures 14C, D,

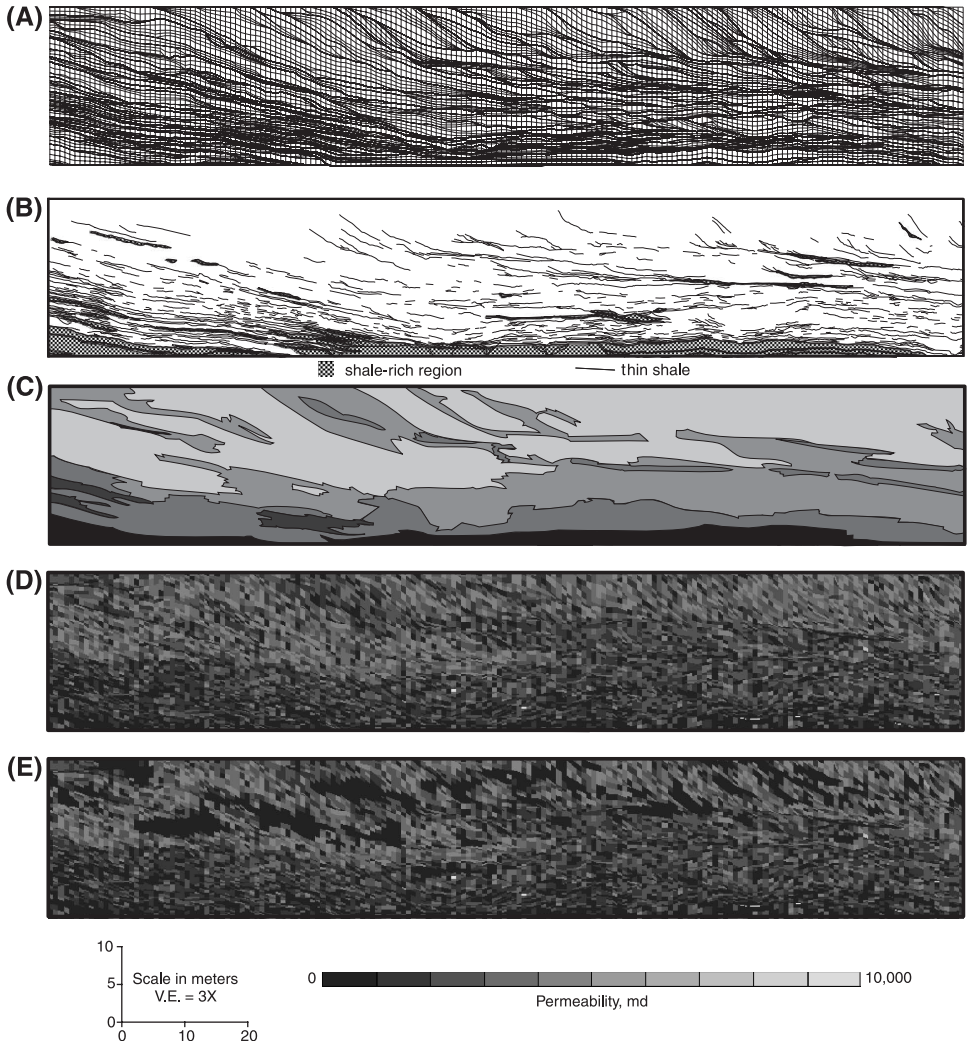

FIGURE 14. Grid and permeability distributions for flow models. (A) The cornerpoint simulation grid conforms to the bedding observed in the outcrop exposure (Figure 4C). (B) Bed-draping shales were mapped (Figure 4F) and included as separate features using transmissibility multipliers rather than block properties. Gray-shaded areas (near the base of the outcrop) indicate shale-rich zones. (C) In some models, permeabilities were assigned using the geometric mean permeability for each facies. (D) In other models, semivariograms (e.g., Figure 7) were used to create sequential Gaussian simulations of the permeability distribution. (E) Calcite concretions were added to the permeability model based on outcrop observations (Figure 4E). Concretion permeability is 0.1 md (Willis and White, 2000).

15B, C), and the displacement is stable (Dake, 1978). The upscaled permeability is nearly the same, whether permeability is assigned by facies or by geostatistical simulation (2.4% difference). Thus, for waterflood displacements through this tide-influenced sandstone, geometric averaging in facies is sufficiently accurate at the horizontal scale of about 400 m.

Low-permeability inclined shales have a pronounced effect on flow patterns. They shunt flow along the clinoforms (Figures 14B, 15D). Compared to the case without shales (Figure 15C), the shales reduce the upscaled permeability by 27% (to 1200 md) and recovery efficiency by 16%. Some shale effects depend on flow direction. For basinward-directed flow, both gravity and shale inclination cause the water to flow lower in the section. If the displacement direction is landward (opposite to bed dip), shale shunting and gravity forces on the water are opposed: the shales push water upward, whereas gravity draws the water downward. The upward coarsening of lithofacies also draws fluids out of the base of the sandstone body (Figure 15B). In combination, lithofacies trend, gravity segregation, and inclined shales lower recovery efficiency by 4% for updip-directed flow compared with downdip-directed flow (Willis and White, 2000). This effect varies with flow velocity. Although small-scale relative permeability is not directional, the reservoir architecture causes waterflood behavior to depend on flow direction. Therefore, upscaled relative permeability is directional.

The concretions were included as altered regions in the permeability grid (Figure 14E). The locations of concretions in this grid were taken directly from outcrop observations. Upscaled permeability is dramatically reduced because the concretions occur preferentially in the highest-permeability part of the sandstone body (Figure 14E). In this example, a model based on depositional lithofacies alone significantly overestimates upscaled permeability (1200 md without concretions versus 670 md with concretions; Willis and White, 2000). Therefore, it is important to include diagenetic factors in detailed reservoir models. Although concretions make flow paths more tortuous (compare Figure 15D, E), the reduction of recovery efficiency caused by concretions (6%) is modest compared to the reduction in permeability.

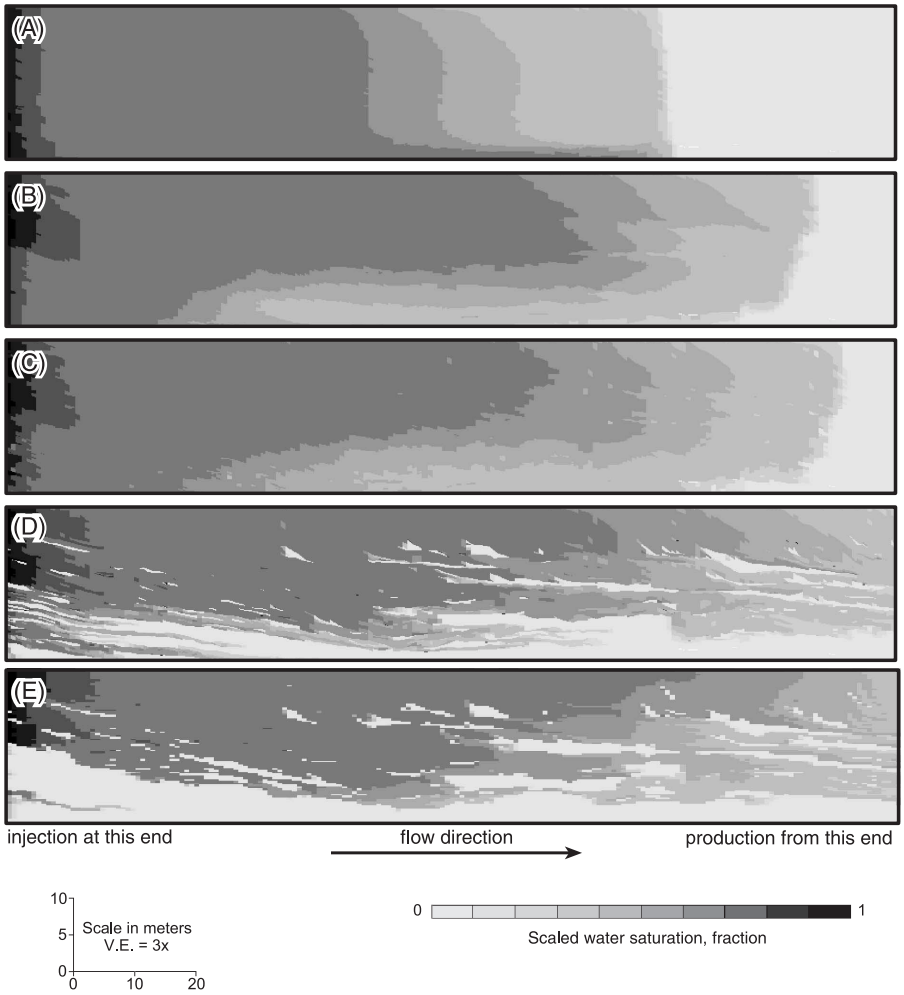

FIGURE 15. Effects of heterogeneities on flow. All models are for a two-dimensional water-displacing-oil simulation, with injection over the full vertical interval on the left and production from the full vertical interval on the right. The water saturation after one-half pore volume of water injection is shown in all figures. (A) In a homogeneous model, gravity draws water toward the bottom of the sandstone body. (B) If permeability is assigned by facies (Figure 14C), viscous forces draw oil upward into higher-permeability regions near the top of the model, counter to gravity forces. (C) Intrafacies variability of permeability simulated geostatistically (Figure 14D) changes the front shape only slightly (compare with B). (D) Shales (Figure 14B) shunt flow downward along the clinoforms and make sweep less uniform. This model uses geostatistical permeability distributions (Figure 14D). (E) Calcite concretions decrease upscaled permeability and make sweep less uniform. This model includes shales (Figure 14B) and geostatistical permeability assignment (Figure 14E; Willis and White, 2000).

Upscaling Complex Geologic Models

Many petrophysical measurements and geologic features are too fine to be included explicitly in the coarse grids that conventionally are used for field-scale performance prediction. However, these data should be integrated into predictive models. Consequently, the effects of these features must be averaged or upscaled. An upscaling method has been formulated using the Frewens sandstone data set as a test case.

Upscaled properties can be derived from fine-scale properties by semianalytic approximations (e.g., Li et al., 1999), limiting approximations based on flow regimes (e.g., Coats et al., 1971; Pickup, 1998) or flow simulation (Kyte and Berry, 1975). The upscaled properties generally depend not only on the pattern of geologic heterogeneity but also on factors including flow velocity, grid-block size, and boundary conditions (Durlofsky, 1997). The dependence of upscaled properties on flow rate and geologic variability causes difficulties when upscaling: upscaled fractional flow functions are different for every grid block and, in general, change if the flow velocity or pressure field changes. Usually, the modeling team chooses a small subset of grid blocks that are ostensibly representative of the range of reservoir heterogeneity and simulates flow subject to boundary conditions that are considered representative of the as-yet unknown large-scale flow patterns. The modeling team then uses the upscaled properties (computed for a few grid blocks and for a few of the manifold possible flow conditions) throughout the reservoir simulation grid.

Response surfaces provide an alternative approach: the variations of upscaled properties caused by geologic and engineering factors are included explicitly. Response-surface models compute upscaled properties appropriate for the heterogeneity of each grid block and local flow conditions based on a small set of simulations chosen by experimental design. After performing a relatively small set of flow simulations (in this study, about 100), the properties for all coarse grid blocks in a field-scale model (often 10,000 or more blocks) are estimated from the response surfaces. Response-surface models are simple polynomials instead of complex phenomenological models. Although they are approximate and empirical, response-surface models are quicker and less expensive than numerical simulation. Experimental design and response-surface methods

Table 1. Factors used in upscaling study (Narayanan, 1999).

Factor	*Raw factor, f_i*	*Factor range, f*		
		Minimum	*Center*	*Maximum*
1) Facies quality	$f_1 = \frac{\sum_{i=4}^{5} h_i}{\sum_{i=1}^{5} h_i}$, h_i = thickness of facies i	0.25	0.5	0.75
2) Shale resistance	$f_2 = \frac{h_{sh}}{k_{sh}}$, h_{sh} = shale thickness (ft), k_{sh} = shale permeability (md)	1	10	100
3) Cement permeability	$f_3 = k_c$ (md)	2.5	25	250
4) Structural dip	f_4 = dip (degrees)	−10	0	10
5) Injection rate	$f_5 = q_w$ (STB/day)		1500	15,000

have been used widely in process design and optimization (Box and Draper, 1987), and reservoir engineers have used the methods for steamflood design (Chu, 1990), uncertainty analysis (Damsleth et al., 1992), sensitivity analysis (Kjønsvik et al., 1992), upscaling (Narayanan, 1999), regression (Eide et al., 1994), parameter estimation (White et al., 2001), and integrated project management (Begg et al., 2001).

The uncertain or variable geologic and engineering parameters (e.g., concretion permeability and injection rate) are the factors. Combinations of factor settings or values (e.g., low concretion permeability and high injection rate) are selected by experimental design. The goal of experimental design is to choose the smallest possible set of factor combinations that accurately describes flow behavior of the model over the ranges of all factors. There are many experimental designs, including two-level factorials (Kjønsvik et al., 1992), D-optimal designs (Damsleth et al., 1992), and Box-Behnken designs (Narayanan, 1999). The analysis presented below uses a Box-Behnken design (Box and Behnken, 1960).

The sandstone-body scale models were upscaled with flow simulations and response-surface models. The 13,000-block model was upscaled in one step to a single coarse block (Narayanan, 1999; Narayanan et al., 1999). Five geologic and engineering factors were considered in the design (Table 1): (1) the facies-specific permeability was idealized as a band of regions parallel to the reservoir top and bottom, and the facies proportions were varied; (2) shale resistance (thickness divided by permeability) was varied; (3) concretion permeability was varied; (4) the grid was rigidly rotated to assess the effects of structural dip; and (5) injection rate was varied.

The flow simulation results are responses; in this study, the responses included upscaled permeability and upscaled relative-permeability parameters. The upscaled permeability and relative permeability were estimated from reservoir simulation models. The upscaled absolute (or single-phase) permeability was computed by the pressure-solver method (Desbarats, 1987). The upscaled relative (or two-phase) permeability was computed from the simulated pressure, water production, and oil production versus time (Johnson et al., 1959). Corey equations were fit to the computed relative permeabilities. Finally, response-surface models were derived for the parameters of the Corey equations to estimate upscaled relative permeability (Narayanan, 1999). Response surfaces are fit using stepwise linear regression (Myers and Montgomery, 1995). The fit of the response surfaces to the simulation results was very good ($R^2 > 0.98$). Examples of response surfaces for average permeability and a relative permeability parameter are shown in Figure 16. The surfaces are two-dimensional slices through the five-dimensional factor space. The surfaces are not linear; this complexity justifies use of the Box-Behnken design instead of the simpler two-level factorial (which is limited to linear response models). These response models explicitly relate rather abstract parameters such as the curvature of the upscaled relative permeability curves to geologic and engineering factors such as shale resistance and flow rate (Figure 16D). Whereas intuition might serve to guide formulation of heuristics for upscaling single-phase permeability, the estimation of relative permeability parameters must rely on computations.

Given these response-surface models, upscaled properties can be computed efficiently. For example, the structural dip and percentage of high-quality facies could be estimated from maps, the flow velocity could be derived from a streamline simulation, and shale and concretion permeabilities could be drawn from prior distributions. The response-surface models then can be used to compute the upscaled single-phase or upscaled relative permeability.

An example of flow predictions from the response surfaces illustrates the accuracy of this approach. Upscaled relative permeabilities were estimated from the response-surface models for extreme values of all

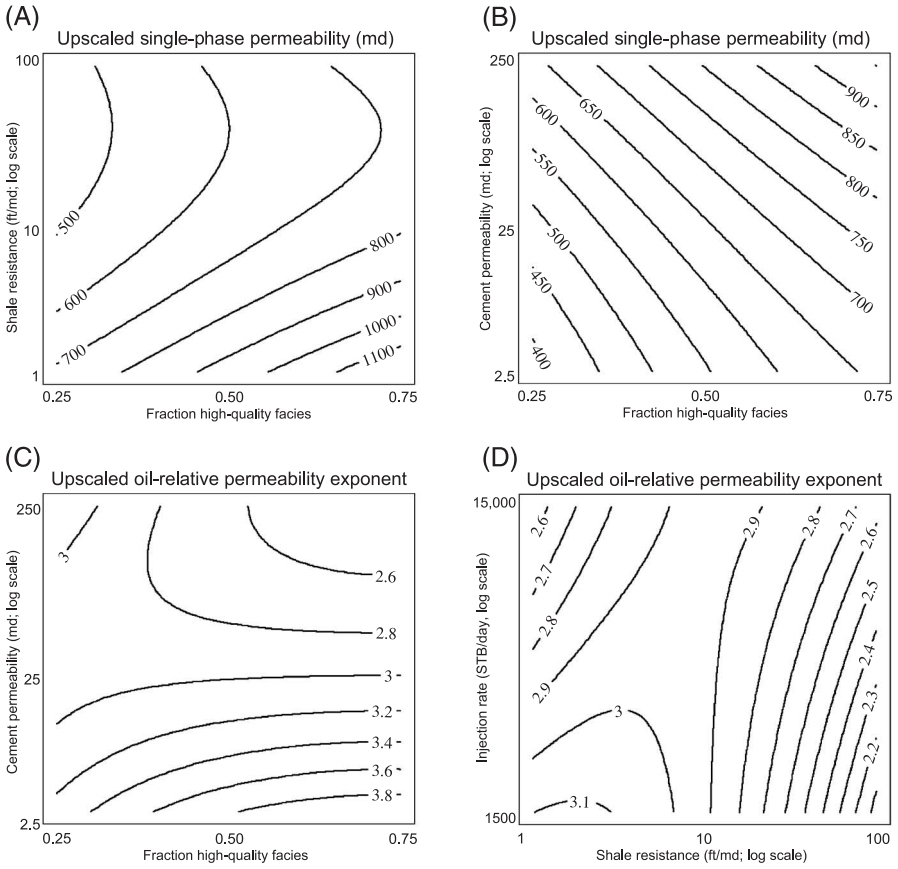

FIGURE 16. Response surfaces for upscaled flow properties. All surfaces are based on five-dimensional response surfaces for the five factors listed in Table 1. In these plots, all factors that are not varied are set at their centerpoint value. (A) Upscaled single-phase permeability decreases as shale resistance increases and increases with the fraction of good-quality facies (facies 4 and 5). (B) Upscaled permeability also is related to concretion permeability. (C) The upscaled oil-relative permeability exponent (the curvature parameter in a Corey model) depends on concretion permeability and the fraction of high-quality facies. (D) The upscaled oil-relative permeability exponent also depends on flow rate and shale resistance (Narayanan, 1999).

factors at a previously unsimulated point. The error in response-surface predictions is maximal at such points (Myers and Montgomery, 1995). The flow behavior was predicted using the Buckley-Leverett model (Dake, 1978) with the upscaled permeability and relative permeabilities. Recovery predicted by the single-block Buckley-Leverett model is compared to the 13,000-grid-block simulation in Figure 17; the match is excellent. For this example, the response surface represents the effects of geologic and engineering factor variation accurately and efficiently.

DISCUSSION

Outcrop studies of reservoir analogs aid reservoir modelers in several ways: by sharpening conceptual understanding, by identifying the most influential factors, and by quantifying deterministically or statistically the spatial distribution of rock bodies, surfaces, and properties. Constructing an analog model, like constructing a reservoir model, is inherently interdisciplinary. Reservoir analog studies require early integration of disciplines to identify the data to be acquired, appropriate formats, and modeling goals. Reservoir engineers must be aware of the realities of field geology, and geologists have to be familiar with the requirements of constructing flow models. The field measurements provide data for flow modeling, and flow modeling identifies sensitivities, which then affect data acquisition priorities. Participation in analog studies affords geoscientists and engineers an opportunity to build and critique reservoir models with denser, higher-resolution, and more accurate data than are typically available for hydrocarbon reservoirs. This experience and testing are often-overlooked benefits of analog studies, in addition to the descriptive and statistical information such studies supply.

It is impossible to find a perfect outcrop analog for a specific reservoir. Outcrop analog studies do not provide a fixed template for reservoir characterization: the genesis of features in the analog must be understood before analog data will provide insights into scales of variations in the subsurface. Outcrop studies allow a broad range of features to be compared with a specific reservoir: the basin position, sequence-stratigraphic setting, hierarchy of facies variations, diagenetic alternation, and rock-property trends. Some features observed in a reservoir might be comparable to those observed in outcrop, whereas others are not. For example, lowstand sandstones in other basins might have gradational bases, eroded tops, and geometries affected by subtle syndepositional seafloor folding (similar to those in the lower Belle Fourche interval examined here), but their internal facies could be quite different. Conversely, reservoir deposits formed in a transgressive estuarine setting may have similar facies but very different large-scale bedding geometry than that produced by the seaward-prograding deltas that formed the Frewens sandstone bodies. Considering too few analog

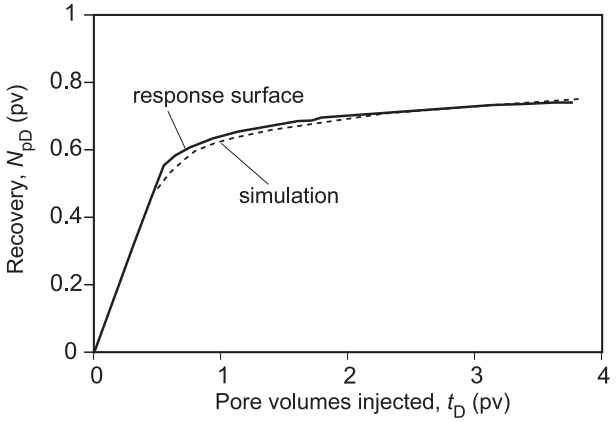

FIGURE 17. Comparison of simulation and response surface predictions. Upscaled flow properties were computed for a previously unsimulated point using response surface models (e.g., Figure 16). Production behavior was predicted at this point using the upscaled properties and Buckley-Leverett theory. Flow was then simulated for the model, and the predictions compare well (Narayanan, 1999).

examples when characterizing a reservoir can lead to misapplication of analog data. Access to a wide range of analog data can help modeling teams avoid this error.

The Frewens sandstone bodies formed in a lowstand setting where low accommodation forced different delta lobes to be offset along strike. In the study area, datums provided by bentonite beds and onlap relationships between adjacent deltas observed in outcrops allowed deposits of different deltas to be distinguished (Bhattacharya and Willis, 2001). In wholly subsurface deposits, these divisions would be more difficult to resolve. Tide-dominated deposition in this setting appears to be localized by the interaction of seabed topography and probably by funneling of tidal currents into shoreline embayments at the start of a regional transgression. Erosion of abandoned deltas by marine currents removed delta-top facies in this setting, and sandstone-body shapes reflect a combination of depositional patterns and subsequent marine erosion (Bhattacharya and Willis, 2001). The major bounding discontinuities defining stratigraphic breaks in lithic trends in the lower Belle Fourche deposits are marine ravinement surfaces. The Frewens tide-influenced sandstone bodies, elongate perpendicular to the shoreline, are positioned adjacent to the underlying lobate sandstone (the Willow Allomember) instead of cutting through the thickest part, as might be expected for a valley cut by the delta-feeding river and then filled during transgression. Without knowledge of the internal facies and bedding geometry, the elongate Frewens sandstone bodies also could be misinterpreted as a transgressive barrier sand deposited along the edge of an abandoned delta lobe or an offshore bar deposited in shelfal water depths.

Large-scale variations in sandstone bodies reflect upward-coarsening facies trends, lateral trends from body axes to margins, and beds dipping parallel to the sandstone-body elongation — all features formed during the seaward progradation of sediments. Barrier sands and offshore bars are generally less heterolithic than the Frewens sandstone bodies and usually have inclined beds approximately perpendicular to sand body elongation. Broad lithologic trends may be easy to define in analogous reservoirs, whereas the lateral extent of smaller-scale variations across beds and sets of beds probably would have to be inferred from vertical logs and analog data. It is notoriously difficult to integrate variograms defined by small-scale features measured in outcrop into subsurface models because of differences in scale and outcrop weathering; nonetheless, the pattern of decreasing correlation range in higher-quality facies probably is representative of tidal deltas. Horizontal and vertical trends in shale length (Figure 10) and the vertical trend in calcite-cemented fraction (Figure 11) probably are very common in analogous reservoirs. There are few other studies that quantify the shape and distribution of calcite concretions in deltaic deposits, but in the absence of reservoir-specific data or other analogs, it is reasonable to use the data presented here to infer subsurface calcite concretion distributions in deltaic sandstone without internal, depositional sources of calcite cement (Dutton et al., 2002). Statistical studies of flow behavior indicate that concretion models must honor the observed trend and mean of cemented fraction, but for these concretions, the inclination is not particularly important (Dutton et al., 2002).

The simulation results must be applied to analogous reservoirs with care because differences in rock and fluid properties cause changes in flow behavior of reservoirs with analogous depositional architecture. That said, it is likely that the highly significant factors, such as shale resistance, would remain highly significant in reservoir-specific studies. Similarly, the intrafacies permeability variations likely will remain relatively insignificant at the scale of hundreds of meters, at least for stable displacements. It is more difficult to speculate about factors with intermediate significance, such as permeability variations at the scale of meters. Overall, the results clearly illustrate the importance of thin, inclined shales, which are often not characterized or modeled carefully. Finally, the methods for assessing sensitivities and upscaling properties can be used in subsurface studies with only slight modifications; such analysis will reveal the key parameters for rock and fluid properties expected in a particular reservoir.

The geostatistical models and flow simulations discussed in this chapter are all two-dimensional. Although intersecting cliff faces (e.g., on Frewens

Castle) provide statistics that are approximately dip- and strike-parallel, adjacent two-dimensional exposures do not provide three-dimensional data. It is difficult to infer anisotropy of shale, concretion, and bed dimensions from two-dimensional outcrop exposures because individual features cannot be accurately mapped throughout the intervening volume. Because the flow models in this study are two-dimensional, they will tend to overestimate the effects of barriers relative to three-dimensional models (Jackson and Muggeridge, 2000).

Like subsurface studies, outcrop analog studies proceed iteratively. In this study, early field observations revealed the prevalence of calcite concretions in the upper sandstone body, and these features were therefore investigated petrographically, mapped on the outcrops, characterized petrophysically, and investigated with flow simulations. Because such concretions cannot be mapped deterministically in the subsurface, geostatistical descriptions for concretion distribution were developed and verified by comparing flow-model predictions for the observed and geostatistically simulated concretion distributions. Similarly, the considerable time required for outcrop permeameter measurements motivated a sensitivity analysis of the importance of these data. That analysis revealed that it is not important to characterize the high-permeability facies in detail, but that the more heterolithic cross-stratified facies (facies 3) should be characterized carefully (Willis and White, 2000). Qualitative observations of trends in shale length led to development of methods to characterize length distributions. Because the outcrop shapes are irregular, the new method had to be accurate for nonrectangular exposures. In characterizing these geologic features, there was repeated feedback between observations and modeling. This flexibility and in-depth analysis is possible only with a team of diverse expertise committed to a multiyear study.

CONCLUSIONS

The Frewens Allomember was deposited in a low-accommodation setting at the distal end of a foreland basin clastic wedge. The location, geometry, and depositional setting of these deposits were controlled by changes in relative sea level and by basin-floor topography associated with the older deltaic deposits and subtle structures. These deposits were interpreted as tide-influenced deltas that prograded into a local shoreline embayment based on a detailed correlation of surfaces and facies trends across regionally extensive outcrops and a three-dimensional grid of subsurface wells. These deltas deposited beds that dip steeply at their landward end and are thinner, more heterolithic, and have lower dip farther offshore.

Grain size, permeability, and porosity were characterized from sedimentologic logs, probe permeameters, and thin sections. Reservoir quality and bed dips increase upward and toward the sandstone-body axis, as expected for a prograding delta. Shale drapes related to tidal modulation of deposition are more common and longer lower in sandstone bodies and toward their margins. Calcite nodules are common in facies with greater primary permeability, particularly along the upper part of the deposit.

Facies distribution, bedding geometry, calcite concretions, shale drapes, structural dip, and flow rate all have significant effects on flow behavior in the Frewens sandstone. Shale effects were particularly significant, making flow nonhorizontal and reducing upscaled permeability. However, intrafacies permeability variations had little influence on upscaled properties on the scale of hundreds of meters. Upscaled relative permeability depends on flow rate and direction, as well as geologic heterogeneity. The dependence of upscaled properties on geologic and engineering factors can be accurately represented using response-surface models.

This study developed a process to improve models of hydrocarbon reservoirs using data from analogous outcrops. The techniques include compilation of a consistent, structured database of geometric and petrophysical data; distribution models for shales only partially exposed in irregularly shaped outcrops; geostatistical models for spatial distribution of calcite concretions; construction of flow models that conform to bedding and honor petrophysical and geostatistical data; experimental design to select simulations; and response-surface methods for sensitivity analysis, upscaling, and parameter estimation. The results of this study include improved stratigraphic and sedimentologic models of tide-influenced reservoirs to aid exploration, mapping, and development; facies models to aid in reservoir characterization; geostatistical descriptions of shale length, permeability distribution, and calcite concretion distribution; methods and results for flow property upscaling; and a sensitivity analysis identifying the most influential geologic features. These results aid in exploring, exploiting, and modeling analogous tide-influenced reservoirs.

ACKNOWLEDGMENTS

This work was sponsored by the Clastic Reservoir Group, Bureau of Economic Geology, the University of Texas at Austin and by the Craft and Hawkins Department of Petroleum Engineering, Louisiana State

University. Financial support to the Clastic Reservoirs Group was provided by Amoco Production, British Petroleum International, Chevron Petroleum Technology, Conoco, Elf Aquitaine Production, Exxon Production Research, Intevep, Japan National Oil, Maxus Energy, Occidental International Exploration and Production, Oryx Energy, OXY USA, Saga Petroleum, Statoil, and Unocal Oil of California. Computer Modeling Group and Schlumberger Technology provided reservoir simulation software. Sharon Gabel, Chris Sweezey, and Charl Brouquet assisted with fieldwork and interpretation. Yugong Gao and Jirapa Skolnakorn helped draft bedding diagrams. Collection of GPR data was funded by a grant from the Advanced Technology Program of the Texas Higher Educational Coordinating Board, and George Tsoflias and James E. Lundy assisted in collection of these data. Djuro Novakovic performed flow simulations. We are grateful to Sharon Gabel for comments on an earlier draft of this paper, and to Bryan Bracken, Paul M. (Mitch) Harris, and F. Jerry Lucia for their insightful reviews for AAPG. We dedicate this work to the late Charl Brouquet, whose friendship, enthusiasm, and energy during fieldwork are greatly missed.

REFERENCES CITED

Ambrose, W. A., E. R. Ferrer, S. P. Dutton, F. P. Wang, A. Padron, W. Carrasquel, J. S. Yeh, and N. Tyler, 1995, Production optimization of tide-dominated deltaic reservoirs of the lower Misoa Formation (lower Eocene), LL-652 area, Lagunillas field, Lake Maracaibo, Venezuela: University of Texas at Austin, Bureau of Economic Geology Report of Investigations no. 226, 46 p.

Barlow, J. A., and J. D. Haun, 1966, Regional stratigraphy of Frontier Formation and relation to Salt Creek field, Wyoming: AAPG Bulletin, v. 50, p. 2185–2196.

Barton, M. D., 1994, Outcrop characterization of architecture and permeability structure in fluvial-deltaic sandstones within a sequence-stratigraphic framework, Cretaceous Ferron sandstone, Utah: Ph.D. dissertation, University of Texas at Austin, 260 p.

Begg, S. H., and P. R. King, 1985, Modelling the effects of shales on reservoir performance: Calculation of effective permeability: 1985 Society of Petroleum Engineers Reservoir Simulation Symposium, Dallas, Texas, February 10–13; SPE Paper no. 13529, p. 331–344.

Begg, S. H., R. B. Bratvold, and J. M. Campbell, 2001, Improving investment decisions using a stochastic integrated asset model: 2001 Society of Petroleum Engineers Annual Technical Conference and Exhibition, New Orleans, September 30–October 3, SPE Paper no. 71414, CD-ROM, 16 p.

Bhattacharya, J. P., and B. J. Willis, 2001, Lowstand deltas in the Frontier Formation, Powder River Basin, Wyoming: AAPG Bulletin, v. 85, p. 261–294.

Box, G. E. P., and D. W. Behnken, 1960, Some new three level designs for the study of quantitative variables: Technometrics, v. 2, no. 4, p. 455–475.

Box, G. E. P., and N. R. Draper, 1987, Empirical model building and response surfaces: New York, Wiley, 669 p.

Brandsæter, I., P. S. Ringrose, C. T. Townsend, and S. Omdal, 2001, Integrated modeling of geological heterogeneity and fluid displacement: Smørbukk gas-condensate field, offshore Mid-Norway: 2001 Society of Petroleum Engineers Reservoir Simulation Symposium, Houston, Texas, February 11–14, SPE Paper no. 66391, CD-ROM, 8 p.

Caers, J. K., S. Srinivasan, and A. G. Journel, 2000, Geostatistical quantification of geological information for a fluvial-type North Sea reservoir: Society of Petroleum Engineers Reservoir Evaluation and Engineering, v. 3, no. 5, p. 457–467.

Chu, C. F., 1990, Prediction of steamflood performance in heavy oil reservoirs using correlations developed by factorial design method: Society of Petroleum Engineers 60th California Regional Meeting, Ventura, California, SPE Paper no. 20020, p. 67–78.

Coats, K. H., J. R. Dempsey, and J. H. Henderson, 1971, The use of vertical equilibrium in two-dimensional reservoir performance: Society of Petroleum Engineers Journal, v. 11, no. 1, p. 63–71.

Computer Modeling Group, 1999, IMEX Version 1999 User's Guide, Calgary, Alberta, Canada.

Corbeanu, R. M., K. Soegaard, R. B. Szerbiak., J. B. Thurmond, G. A. McMechan, D. Wang, S. Snelgrove, C. B. Forster, and A. Menitove, 2001, Detailed internal architecture of a fluvial channel sandstone determined from outcrop, cores, and 3-D ground penetrating radar: Example from the middle Cretaceous Ferron sandstone, east-central Utah: AAPG Bulletin, v. 85, p. 1583–1608.

Dake, L. P., 1978, Fundamentals of reservoir engineering: Amsterdam, Elsevier Scientific Publishing, 443 p.

Damsleth, E., A. Hage, and R. Volden, 1992, Maximum information at minimum cost: A North Sea field development study with experimental design: Journal of Petroleum Technology, v. 44, no. 12, p. 1350–1360.

Desbarats, A. J., 1987, Numerical estimation of effective permeability in sand-shale formations: Water Resources Research, v. 23, no. 2, p. 273–286.

Deutsch, C. V., and A. G. Journel, 1998, GSLIB: Geostatistical software library and user's guide: New York, Oxford University Press, 369 p.

Durlofsky, L. J., 1997, Use of higher moments for the description of upscaled, process independent relative permeabilities: Society of Petroleum Engineers Journal, v. 2, no. 4, p. 474–485.

Dutton, S. P., B. J. Willis, C. D. White, and J. P. Bhattacharya, 2000, Outcrop characterization of reservoir quality and interwell-scale cement distribution in a tide-influenced delta, Frontier Formation, Wyoming, USA: Clay Minerals, v. 35, p. 95–105.

Dutton, S. P., C. D. White, B. J. Willis, and D. Novakovic,

2002, Calcite cement distribution and its effect on fluid flow in a deltaic sandstone, Frontier Formation, Wyoming: AAPG Bulletin, v. 86, p. 2007–2021.

Dyman, T. S., E. A. Merewether, C. M. Molenaar, W. A. Cobban, J. D. Obradovich, R. J. Weimer, and W. A. Bryant, 1994, Stratigraphic transects for Cretaceous rocks, Rocky Mountains and Great Plains Regions, *in* M. V. Caputo, J. A., Peterson, and K. J. Franczyk, eds., Mesozoic systems of the Rocky Mountain region, USA: Rocky Mountain Section, Society for Sedimentary Geology (SEPM), p. 365–292.

Eide, A. L., L. Holden, E. Reiso, and S. Aanononsen, 1994, Automatic history matching by use of response surfaces and experimental design: 1994 European Conference on the Mathematics of Oil Recovery, Roros, Norway, June 7–10, 14 p.

Geehan, G., and J. Underwood, 1993, The use of length distributions in geological modeling: The geological modeling of hydrocarbon reservoirs and outcrop analogues, *in* S. S. Flint and I. D. Bryant, eds., International Association of Sedimentologists Special Publication 15: Oxford, Blackwell Scientific Publications, p. 205–212.

Goggin, D. J., 1993, Probe permeametry: Is it worth the effort?: Marine and Petroleum Geology, v. 10, p. 299–308.

Haldorsen, H. H., and L. W. Lake, 1984, A new approach to shale management in field scale simulation models: Society of Petroleum Engineers Journal, v. 24, no. 4, p. 447–457.

Hewett, T. A., and R. A. Behrens, 1993, Considerations affecting the scaling of displacements in heterogeneous permeability distributions: Society of Petroleum Engineers Formation Evaluation, v. 7, p. 258–266.

Honarpour, M., L. F. Koederitz, and H. A. Harvey, 1982, Empirical equations for estimating two-phase relative permeability in consolidated rock: Journal of Petroleum Technology, v. 34, p. 2905–2908.

Jackson, M. D., and A. H. Muggeridge, 2000, Effects of discontinuous shales on reservoir performance during horizontal waterflooding: Society of Petroleum Engineers Journal, v. 5, no. 4, p. 446–455.

Johnson, E. F., D. P. Bossler, and V. O. Naumann, 1959, Calculation of relative permeability from displacement experiments: Transactions of the American Insitute of Mining, Metallurgical, and Petroleum Engineers, v. 216, p. 370–372.

Kjønsvik, D., T. Jacobsen, and A. Jones, 1992, The effects of sedimentary heterogeneities on production from shallow marine reservoirs— what really matters?: Society of Petroleum Engineers 1992 European Petroleum Conference, London, SPE Paper no. 28445, p. 27–40.

Kurniawan, A. Syaefuddin, T. Bailey, and H. H. Santoso, 2001, Geological modelling: Backbone in developing a mature oil field (Jorang field case): 2001 Society of Petroleum Engineers Asia Pacific Oil and Gas Conference and Exhibition, Jakarta, Indonesia, April 17–19, SPE Paper no. 68640, CD-ROM, 6 p.

Kyte, J. R., and D. W. Berry, 1975, New pseudofunctions to control numerical dispersion: Society of Petroleum Engineers Journal, v. 15, no. 4, p. 269–285.

Lerch, C. S., K. W. Bramlett, W. H. Butler, J. N. Scales, and T. B. Stroud, 1996, Integrated 3-D reservoir-modeling at Ram-Powell field: A turbidite reservoir in the eastern Gulf of Mexico: 1996 Society of Petroleum Engineers Annual Technical Conference and Exhibition, Denver, Colorado, October 6–9, SPE Paper no. 36729, p. 477–492.

Li, D., B. Beckner, and A. Kumar, 1999, A new efficient averaging technique for scale-up of multimillion-cell geologic models: 1999 Society of Petroleum Engineers Annual Technical Conference and Exhibition, Houston, Texas, October 3–6, SPE Paper no. 56554, CD-ROM, 15 p.

Matheron, G., H. Beucher, C. de Fouquet, and A. Galli, 1987, Conditional simulation of the geometry of fluvio-deltaic reservoirs: 62nd Annual Technical Conference and Exhibition of the Society of Petroleum Engineers, Dallas, Texas, September 27–30, SPE Paper no. 16753, p. 591–599.

McGooky, D. P., J. D. Haun, L. A. Hale, H. G. Goodell, D. G. McCubbin, R. J. Weimer, and G. R. Wulf, 1972, Cretaceous systems, *in* W. W. Mallory, ed., Geological atlas of the Rocky Mountain region, United States of America: Denver, Colorado, Rocky Mountain Association of Geologists, p. 190–228.

McMechan, G. A., G. C. Gaynor, and R. B. Szerbiak, 1997, Use of ground-penetrating radar for 3-D sedimentological characterization of outcrop analogs: Geophysics, v. 62, p. 786–796.

Merewether, E. A., W. A. Cobban, and E. T. Cavanaugh, 1979, Frontier Formation and equivalent rocks in eastern Wyoming: The Mountain Geologist, v. 16, p. 67–101.

Myers, R. H., and D. C. Montgomery, 1995, Response surface methodology: Process and product optimization using designed experiments: New York, Wiley, 700 p.

Narayanan, K., 1999, Applications for response surfaces in reservoir engineering: Unpublished M.S. thesis, University of Texas at Austin, 90 p.

Narayanan, K., C. D. White, L. W. Lake, and B. J. Willis, 1999, Response surface methods for upscaling heterogeneous geologic models: 15th Society of Petroleum Engineers Symposium on Reservoir Simulation, Houston, Texas, February 14–17, SPE Paper no. 51923, p. 333–334.

Nissen, S. E., J. M. Combes, and A. G. Nekut, 1999, Acquisition, processing, and analysis of shallow, high-resolution seismic data from the outer continental shelf and upper slope, offshore Louisiana: Journal of Sedimentary Research, v. 69, no. 2, p. 300–316.

Pickup, G. E., 1998, Steady state upscaling: From lamina-scale to full-field model: 1998 Society of Petroleum Engineers European Conference, The Hague, The Netherlands, October 20–22, SPE Paper no. 50628, p. 527–535.

Prats, M., 1972, The influence of oriented arrays of thin impermeable shale lenses or of highly conductive

natural fractures on apparent permeability anisotropy: Journal of Petroleum Technology, v. 24, p. 1219–1222.

Rossini, C., F. Brega, L. Piro, M. Rovollini, and G. Spotti, 1994, Combined geostatistical and dynamic simulations for developing a reservoir management strategy: A case history: Journal of Petroleum Technology, v. 46, p. 979–985.

Schlumberger Technology, 1997, Eclipse 100 Reference Manual, unpaginated.

Tillman, R. W., and E. A. Merewether, 1994, Field guide for valley-fill, estuarine, and shelf ridge sandstones, mid-Cretaceous Frontier Formation, central Wyoming: Denver, Colorado, AAPG Annual Meeting Field Trip Guidebook, 90 p.

Tillman, R. W., and E. A. Merewether, 1998, Bayhead-delta and estuary-mouth bars of early Cenomanian age in the mid-Cretaceous Frontier Formation, Wyoming (abs): AAPG Annual Meeting Program, 4 p.

Tye, R. S., J. P. Bhattacharya, J. A. Lorsong, S. T. Sindelar, D. G. Knock, D. D. Puls, and R. A. Levinson, 1999, Geology and stratigraphy of fluvio-deltaic deposits in the Ivishak Formation: Applications for development of Prudhoe Bay field, Alaska: AAPG Bulletin, v. 83, p. 1588–1623.

Visser, C. A., and A. G. Chessa, 2000, A new method for estimating lengths of partially exposed features: Mathematical Geology, v. 32, no. 1, p. 109–126.

Walderhaug, O., P. A. Bjørkum, and H. M. Nordgård Bolås, 1989, Correlation of calcite-cemented layers in shallow-marine sandstones of the Fensfjord Formation in the Brage field, *in* J. D. Collinson, ed., Correlation in hydrocarbon exploration: London, Graham & Trotman, p. 367–375.

White, C. D., and M. D. Barton, 1999, Translating outcrop data to flow models, with applications to the Ferron sandstone: Society of Petroleum Engineers Reservoir Evaluation and Engineering, v. 2, no. 4, p. 341–350.

White, C. D., and B. J. Willis, 2000, A method to estimate length distributions from outcrop data: Mathematical Geology, v. 32, no. 4, p. 389–419.

White, C. D., B. J. Willis, and K. Narayanan, 2001, Identifying and estimating significant geologic parameters with experimental design: Society of Petroleum Engineers Journal, v. 6, no. 3, September, p. 311–324.

Willis, B. J., 1998, Permeability structure of a compound valley fill in the Cretaceous Fall River Formation of South Dakota: AAPG Bulletin, v. 82, p. 206–227.

Willis, B. J., and C. D. White, 2000, Quantitative outcrop data for flow simulation: Journal of Sedimentary Research, v. 70, p. 788–802.

Willis, B. J., J. P. Bhattacharya, S. L. Gabel, and C. D. White, 1999, Architecture of a tide-influenced delta in the Frontier Formation of central Wyoming: Sedimentology, v. 46, p. 667–688.

Worden, R. H., and J. M. Matray, 1998, Carbonate cement in the Triassic Chaunoy Formation of the Paris Basin: Distribution and effect on flow properties, *in* S. Morad, ed., Carbonate cementation in sandstones: International Association of Sedimentologists Special Publication 26, p. 163–177.